Contributions to Mineralogy and Petrology (2023) 178:12
https://doi.org/10.1007/s00410-022-01983-w

ORIGINAL PAPER

High-K andesites as witnesses of a continental arc system in the Western Alps, Italy: constraints from HFSE and Hf–Nd–Sr–Pb–O isotope systematics

S. Jung[1] · J. A. Pfänder[2] · O. Nebel[3] · M. Willbold[4] · S. Hoernes[5] · J. Berndt[6] · A. Pack[4]

Received: 21 April 2022 / Accepted: 8 December 2022 / Published online: 24 January 2023

Abstract

Geochemical and isotopic data are presented for ~ 32 Ma-old high-K andesites and dacites from the Alpine Chain. The samples consist of plagioclase, amphibole, titanomagnetite and rare biotite and quartz. Geochemical and isotope data indicate that slab-derived fluids, sediment melts and presumably AFC processes involving continental crust played a key role in the petrogenesis of the high-K rocks. A contribution of fluids is suggested based on the overall enrichment of large-ion lithophile elements and related high Ba/La, Ba/Zr, Ba/Th, Ba/Nb and Pb/Nd, sometimes distinctively higher than average continental crust. Positively correlated Ba/Nb–Th/Nb relationships, low Ce/Pb, low Nb/U and a negative correlation of Pb isotopes with Ce/Pb and Nb/U and positive Δ 7/4 and Δ 8/4 values similar to GLOSS imply the additional involvement of a sediment-derived melt. Negatively correlated Nb/Ta–Zr/Hf ratios at overall low Nb/Ta (13–7.5) are best explained by parental magma differentiation involving amphibole and biotite in a continental arc system. The samples have moderately unradiogenic Nd (εNd: – 2.0 to – 6.7) and radiogenic $^{87}Sr/^{86}Sr$ isotope compositions (0.7085–0.7113), moderately radiogenic Pb isotope compositions ($^{206}Pb/^{204}Pb$: 18.50–18.72; $^{207}Pb/^{204}Pb$: 15.59–15.65; $^{208}Pb/^{204}Pb$: 38.30–38.67), and elevated $\delta^{18}O$ values (+ 6.5 to + 9.1 ‰). Epsilon Hf isotope values range from + 2.5 to – 4.0. Negative εHf(*t*) and εNd(*t*) values and $^{206}Pb/^{204}Pb$ ratios are correlated with elevated K_2O abundances that indicate enrichment in K_2O is related to AFC processes. The offset of εHf at a given εNd points to involvement of aged garnet-bearing crustal lithologies. The latter feature is qualitatively consistent with modification of unexposed primary basaltic andesites by AFC processes involving deep crustal material. In conclusion, in an Alpine context, inferred unexposed primitive high-K basaltic to andesitic melts are generated in the mantle wedge through fluid infiltration from the descending slab where fluids may have caused also partial melting of sedimentary rocks that mixed with evolving andesite–dacite compositions towards shallow-level intrusive and extrusive rocks. High-K and related trace element and isotope features thus result from a combination of already elevated values with participation of fluids and melts and probably AFC processes.

Keywords High-K andesites · Trace elements · Nb–Ta–Zr–Hf systematics · Nd–Sr–Pb–Hf–O isotopes · Alpine chain

Communicated by Hans Keppler.

✉ S. Jung
stefan.jung@uni-hamburg.de

[1] Fachbereich Erdsystemwissenschaften, Mineralogisch-Petrographisches Institut, Universität Hamburg, Grindelallee 48, 20146 Hamburg, Germany

[2] Institut für Geologie, Technische Universität Bergakademie Freiberg, Gustav-Zeuner-Str. 12, 09599 Freiberg, Germany

[3] School of Earth, Atmosphere and Environment, Monash University, Clayton, VIC 3800, Australia

[4] Geowissenschaftliches Zentrum, Georg-August-Universität Göttingen, Goldschmidtstraße 1, 37073 Göttingen, Germany

[5] Mineralogisch-Petrologisches Institut der Universität Bonn, Poppelsdorfer Schloß, 53115 Bonn, Germany

[6] Institut für Mineralogie, Universität Münster, Corrensstr. 24, 48149 Münster, Germany

Introduction

Igneous rocks associated with subduction-related tectonic settings commonly belong to distinct magmatic series ranging from high-Al basalt to rhyolite, but often differ considerably in their K_2O content. It is commonly accepted that multiple sources are involved in andesite generation and subsequent interaction between melts derived from these sources are required to explain the geochemical and isotopic diversity of subduction-related volcanic rocks (Arculus and Powell 1986; Ellam and Hawkesworth 1988; Stolz et al. 1990; Hawkesworth et al. 1993). Probably, the volumetrically most important component is the mantle wedge that can have geochemical and isotopic compositions ranging from normal mid-ocean ridge basalts (N-MORB) source mantle (Perfit et al. 1980) or even depleted MORB (D-MORB) source mantle (McCulloch and Gamble 1991; Woodhead et al. 1993; Elliot et al. 1997) to highly enriched ocean island basalt-type (OIB) source mantle (Morris and Hart 1983; Stolz et al. 1990; Edwards et al. 1994; Turner et al. 2017), however, the composition of the down-going slab may also be important. A second critical aspect might be the temperature of the mantle wedge and the down-going slab, its sediment load, subduction angle and velocity. These parameters affect the type and interplay of distinct fluids and melts derived from them (Turner et al. 2016). The elemental and isotopic composition of many subduction-related volcanic complexes requires further additional involvement of other components, including fluids of subducted oceanic crust and associated sedimentary rocks or partial melts thereof (Kay 1980; White and Duprè 1986; Ellam and Hawkesworth 1988; McDermott et al. 1993; Gamble et al. 1996; Price et al. 1999; Vroon et al. 1993, 2001). In this context, varying contributions of the subduction-related components to the source region of arc magmas, the transfer mechanisms of specific elements from the slab to the sub-arc mantle and the composition and amount of the subducted sediment are important parameters (Ellam and Hawkesworth 1988; Elliot et al. 1997; Plank and Langmuir 1998). Additional modification of arc magmas that usually lead to more enriched isotope compositions may come from interaction with pre-existing continental crust during movement through and stagnation within the crust (Hildreth and Moorbath 1988; Davidson 1987; Davidson and Harmon 1989; Davidson et al. 1990; Ellam and Harmon 1990; Thirlwall et al. 1996). Therefore, based on the numerous important factors that may affect the chemistry of subduction-related volcanic rocks, a universally valid model for the generation of these rocks is precluded.

A series of arc lavas of controversial origin are high-K andesites or shoshonites. Andesites are in general rare in arc settings compared to their basaltic and rhyolitic counterparts (Reubi and Blundy 2009). The enrichment in K (and sometimes Na) is not fully understood as in either scenario of andesite genesis (magma mixing, fractional crystallization with and without assimilation), both, Na and K increase in tandem. However, some andesitic volcanoes develop distinctively high-K contents (Price et al. 1999; Zernack et al. 2012), which require one or more additional processes in the mantle or the crust en route to the surface.

In this contribution, we present mineral data, major and trace element whole-rock compositions and Sr, Nd, Pb, Hf and O isotope data as well as biotite and amphibole Ar–Ar ages for a series of Oligocene high-K subduction-related volcanic rocks from the Southern Alps (Italy). Due to the sparseness of the volcanic centers in the Alps (McCarthy et al. 2021) and pronounced post-orogenic uplift and concomitant erosion, primary volcanic centers are no longer preserved in the Alpine chain, but remnants of subduction-related volcanic rocks occur as large decimeter-sized boulders in molasse-type sedimentary rocks of the Oligocene–Miocene Gonfolite Lombarda Formation (Como, Italy; Gunzenhauser 1985). These boulders may provide the necessary information on the geochemistry and isotope geochemistry of no longer exposed volcanic rocks. Like few subduction-related suites from worldwide occurrences (i.e., lesser Antilles; Nielsen and Marschall 2017), all samples are characterized by radiogenic Sr and Pb isotope compositions, unradiogenic Nd and Hf isotope compositions and moderate to high $\delta^{18}O$ values. The samples range in composition from large-ion lithophile element (LILE)- and light rare-earth element (LREE)-enriched high-K andesites to dacites with a pronounced depletion in HFSE. Based on geochemical and isotope criteria, we will use these samples to constrain the effects of crustal contamination as well as fluid and melt interaction with mantle wedge peridotite on the generation of geochemical and isotopic variability in andesitic lavas.

Sample locality, petrography and mineral composition

In the alpine chain, Eocene to Oligocene igneous rocks are exposed along the several 100 km-long Periadriatic Fault System that strikes E–W. Subduction-related magmatism occurred from ~ 43 Ma to ~ 29 Ma with input of mafic material at ~ 32–29 and ~ 43–40 Ma (Müntener et al. 2021). The first period ceased prior to the collision of Europe and Africa and the later period represents the phase of continental arc magmatism. The latter age range agrees well with the $^{40}Ar/^{39}Ar$ ages of 30.1–32.6 Ma obtained in this study (Table A1), which also fall in the range of ages obtained on the Bergell intrusion (30–32 Ma; von Blankenburg 1992; Oberli et al. 2004; Gianola et al. 2014); an intrusion that is

characterized by high-K magmatic rocks. Numerous authors (Nievergelt and Dietrich 1977; Gautschi and Montrasio 1978; Beccaluva et al. 1979, 1983; Dal Piaz et al. 1979, 1988; Venturelli et al. 1984; Diethelm 1990; von Blanckenburg et al. 1992; Ruffini et al. 1997) reported on the occurrence of andesitic rocks including rare shoshonites from the Alpine chain that occur mostly as dykes and as fragments within post-orogenic sedimentary successions. The Oligocene to Miocene succession of the Gonfolite Lombarda Formation crops out in western Lombardy (Fig. 1). It can be considered as a typical example of a post-orogenic molasse deposit although subsequent work indicates that it more likely represents a clastic wedge infilling a deep foreland basin flanking a zone of continental collision (Gelati et al. 1988). The succession covers a time span from late early Oligocene to early Miocene and consists of clastic sedimentary rocks that were deposited, based on bentic foraminifera and macrofossil evidence, in a deep-sea environment. The Gonfolite Group as part of the Gonfolite Lombarda succession consists at the base of the Como Conglomerate. Within this conglomerate, numerous boulders of granite–granodiorite of the Val Masino–Val Bregglia massif occur as well as numerous boulders of high-grade metamorphic rocks (eclogites, blue schists, mica schists, felsic granulites, mafic granulites, amphibolites) from the crystalline basement of the Alps (Gelati et al. 1988). This formation also yields numerous boulders of volcanic rocks that form the sample basis of this study. These boulders which are elliptical in shape have

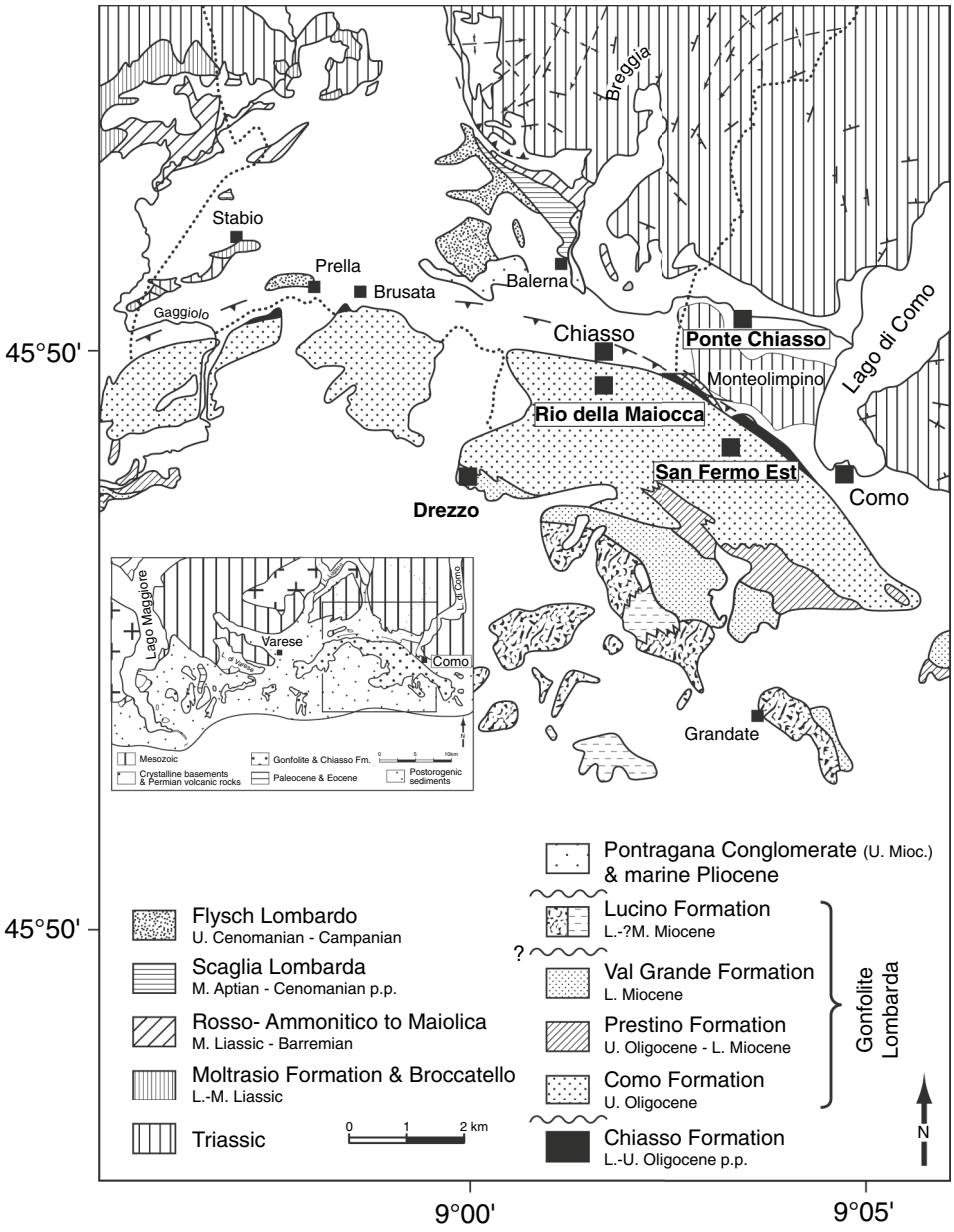

Fig. 1 Occurrence of the Gonfolite Lombarda Group within the Alpine realm and a geological sketch map of the region between Como and Chiasso with sample locations

long axes between 15 and 30 cm and a length to width ratio of 1.5 to 2 and were collected at Rio della Maiocca south of Chiasso, at San Fermo Est and at Ponte Chiasso (Fig. 1).

Typical mineral assemblages of the high-K andesites and dacites consist of plagioclase, amphibole, biotite and titanomagnetite. Mineral compositions are given in Table A2 and element profiles for amphibole are shown in Fig. A1. All samples are highly porphyritic and phenocrysts of plagioclase and amphibole may reach grain sizes up to 2 mm. Amphibole occur as phenocrysts or forms mineral aggregates and can be classified as edenite. Two samples contain large flakes of biotite. Apatite is common and occurs as microphenocrysts. Phenocrysts, microphenocrysts and mineral aggregates are enclosed in a fine-grained, slightly altered groundmass in which primary glass is absent. Euhedral to subhedral plagioclase is usually twinned and its composition ranges from An39 to An58 (Table A2). Zoning is commonly normal, reverse or oscillatory.

Methods

$^{40}Ar/^{39}Ar$ dating was carried out at Argonlabor Freiberg (ALF), TU Freiberg, Germany. Raw-data reduction and time-zero intercept calculations were done using an in-house developed Matlab software package, isochron, inverse isochron and plateau ages have been calculated with the Excel Add-In ISOPLOT 3.7 (Ludwig 2008). Fish Canyon Tuff sanidine was used as flux monitor (28.305 ± 0.036 Ma; Renne et al. 2010) and the decay constants of Renne et al. (2010) served as base for all calculations. A detailed description of the method is given in the appendix and data are given in the online resources. Minerals were analyzed with a JEOL microprobe at the University of Münster, Germany. Operating condition were 15 kV and 5 nA, with a peak counting time of 5 s and a background counting time of 3 s with a beam size of 5–20 µm. The ZAF correction procedure was applied to the data; errors in the major oxides are estimated to be about 1–2%. Representative mineral data are given in Table A2. Whole rock powders were prepared from rock chips free from surface alteration using a jaw crusher, a ball mill and an agate mortar. Major and some trace elements (except for rare-earth elements (REE) and Nb, Ta, Hf, Th and U) were determined on fused lithium-tetraborate glass beads using standard XRF techniques. A more detailed description of the method is given in the appendix and data for certified reference materials are given in Table A3. For some samples, trace element concentrations of Nb, Hf, Ta, Th, and U were determined by isotope dilution inductively coupled mass spectrometry (ID-ICPMS) using a Thermo-Electron ELEMENT 2 high-resolution ICPMS at Max-Planck Institut für Chemie, Mainz. A detailed description of the method can be found in the appendix and in Willbold and Jochum (2005) and data for certified reference materials are given in Table A3. Sr, Nd and Pb isotope analyses were carried out at the Max-Planck-Institut für Chemie at Mainz with a Finnigan MAT 261 multicollector thermal ionization mass spectrometer operating in static mode. A more detailed description of the method can be found in the appendix and data for certified reference materials are given in Table A4. Isotope analyses of Lu and Hf were carried out on a Thermo Fisher® Neptune MC-ICP-MS at U Amsterdam. A more detailed description of the method can be found in the appendix and data for certified reference materials are given in Table A4. Oxygen isotope analyses for samples CS 42, CS 56, CS 66, CS 88, CS 22, CS 39, CS 53, CS 59 and CS 89 were performed at the University of Bonn on ~ 10 mg aliquots of powdered whole-rock samples. Oxygen isotope analyses for samples CS 69, CS 32, CS 54, CS 57, CS 91 and CS 97 were analyzed at Universität Göttingen using infrared (IR) laser fluorination in combination with gas chromatography isotope ratio monitoring gas mass spectrometry. Analytical uncertainties are < 0.2‰. All samples were measured twice and the average of these measurements is given in Table 2. All values are reported as per mil deviations relative to SMOW (Standard Mean Ocean Water) and refer to a certified value of 9.6 ± 0.2‰ for NBS 28. A more detailed description of the method can be found in the appendix and data are given in Table 2.

Results

Ar–Ar ages

For all three samples dated in this study, the reported plateau and inverse isochron ages (Fig. A2) are identical within error, and the initial $^{40}Ar/^{36}Ar$ compositions are indistinguishable from the atmospheric value of 298.6 ± 0.3 (Lee et al. 2006). Therefore, the plateau ages are taken as best estimates for the time of cooling through the ~ 550 °C (amphibole) and ~ 335 °C (biotite) temperature range (cooling temperatures calculated using Mark Brandon's closure program and diffusion datasets of Harrison (1981) and Grove and Harrison (1996) and assuming a cooling rate of 70 °C/Ma and a uniform grain size of 250 µm). The age spectrum of sample CS22 exhibits an excess Ar component present in the low temperature steps, but provides a plateau age of 32.6 ± 0.3 Ma (2σ) from 78.5% of the released ^{39}Ar. K/Ca ratios are fairly constant for the steps comprising the plateau and indicate Ar release from a homogeneous unaltered phase. For sample CS66, low signal intensities cause relatively large errors on the individual temperature steps, therefore, all steps have been used to calculate an age of 32.8 ± 0.7 Ma. The biotite separate from sample CS53 provides a slightly disturbed age spectrum and a somewhat

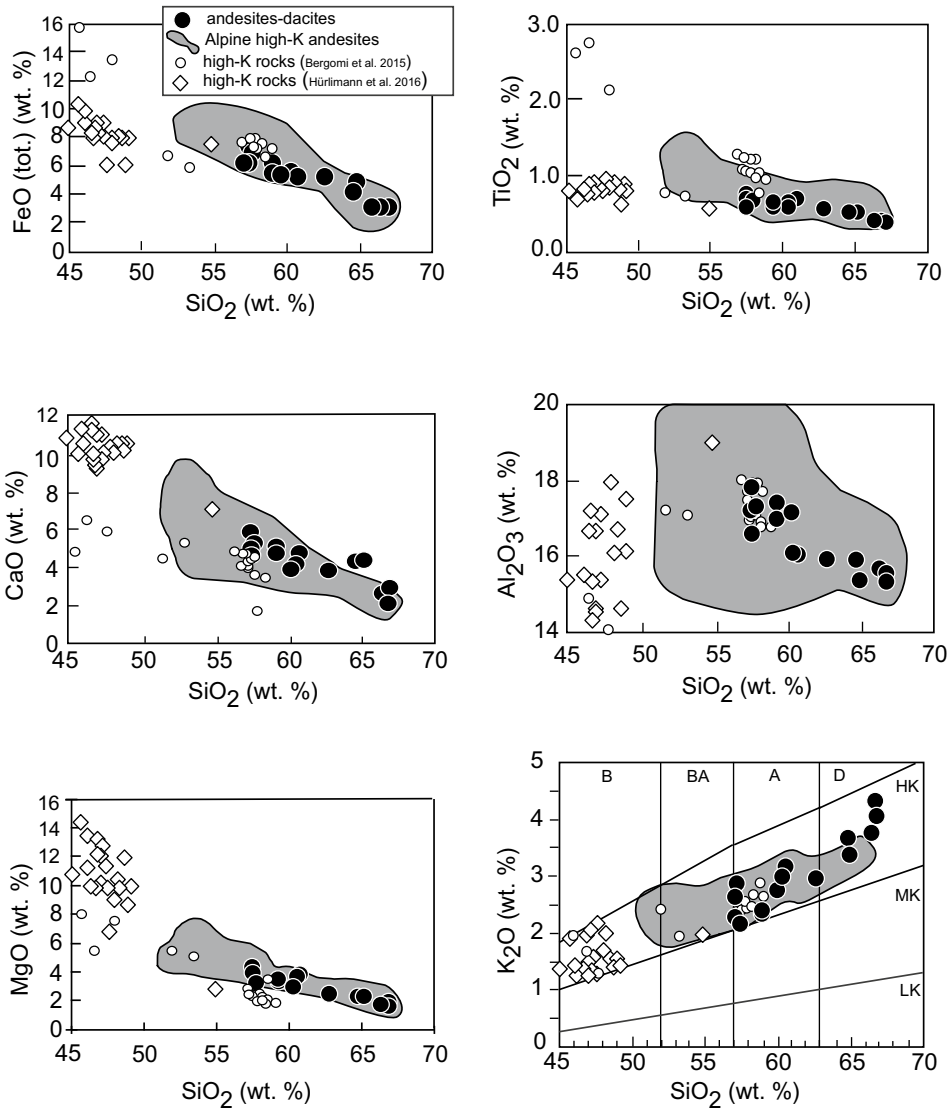

Fig. 2 Major oxide (FeO_{total}, TiO_2, CaO, Al_2O_3, MgO, P_2O_5 and K_2O vs. SiO_2) variation diagrams of the andesites and dacites. B: basalt, BA: basaltic andesite, A: andesite, D: dacite, LK: low-K_2O, CA: calc-alkaline, HK: high-K_2O. Grey field denotes data for other high-K andesites and dacites from the Alps according to Deutsch (1984), Beccaluva et al. (1979), Diethelm (1990), Gautschi and Montrasio (1978), Dal Piaz et al. (1979), (1988) and Ruffini et al. (1997). Reference data for mafic high-K rocks from Hürlimann et al (2016) and Bergomi et al. (2015) are shown for comparison

lower age than the amphiboles of 30.1 ± 0.1 Ma from 95.5% of the released ^{39}Ar. Data are given in the online resources.

Geochemistry

Analytical techniques are given in the Appendix A1. Major element compositions of whole-rock samples are given in Table 1. Selected major elements are plotted against SiO_2 in Fig. 3. According to their K_2O content the samples are classified as high-K andesites and dacites with X_{Mg} (X_{Mg} = molar Mg/molar Mg + molar Fe; all Fe as FeO) ranging from 0.47 to 0.57. SiO_2 ranges from 57.4 to 66.8 wt%. TiO_2, FeO* (all Fe as FeO), MgO, CaO and Al_2O_3 decrease with increasing SiO_2. Na_2O increases weakly from c. 2.7–3.2 wt % in the least evolved samples to c. 3.7 wt. % in the most evolved samples. P_2O_5 concentrations are rather low (0.12–0.21 wt. %) and increase with increasing SiO_2. Trace element compositions are given in Table 1 and are plotted in Fig. 3a and b. Compatible trace elements (Cr, Sc, Ni, and V) are low and constant or weakly positively correlated when plotted against MgO. Incompatible LILE (Rb, Ba, Pb) increase with decreasing MgO although there is considerable scatter among the samples. Strontium shows no correlation with MgO. Other incompatible elements (U, Th) also increase with decreasing MgO. Incompatible HFSE show either no correlation with MgO (Zr, Hf) or increase with decreasing MgO (Nb, Ta). The Nb/Ta ratios range from 7.5 to 13.0 and the Zr/Hf ratios range from 34.3 to 41.5 in which Nb/Ta and Zr/Hf are positively correlated but are uncorrelated to MgO. A chondrite-normalized REE plot for selected samples is shown in Fig. 4. All samples are enriched in LREE relative to the HREE with chondrite-normalized La_n/Yb_n ratios ranging from 3.8 to 12.5. All samples have small to moderate negative Eu anomalies that range from

Table 1 Major and trace element composition of the andesites–dacites. LOI: loss on ignition. Major elements in wt. %. trace elements in ppm

	CS 42	CS 56	CS 66	CS 88	CS 91	CS 69	CS 97	CS 22	CS 39	CS 53	CS 59	CS 89	CS 32	CS 54	CS 57
SiO_2	57.4	57.4	60.2	59.2	57.6	59.2	65.0	60.7	66.4	66.8	64.7	66.7	57.4	62.7	60.4
TiO_2	0.71	0.61	0.56	0.60	0.66	0.58	0.49	0.67	0.37	0.37	0.51	0.38	0.69	0.55	0.64
Al_2O_3	17.3	17.8	17.2	17.0	17.4	17.5	15.4	16.1	15.7	15.5	15.9	15.3	16.6	15.9	16.1
Fe_2O_3	3.14	3.19	2.39	3.28	7.24	6.00	4.68	1.91	1.13	1.06	2.15	1.34	6.69	5.61	6.00
FeO	4.08	3.04	3.05	2.79	0.00	0.00	0.00	3.31	1.98	1.97	2.06	1.89	0.00	0.00	0.00
MnO	0.10	0.06	0.07	0.09	0.09	0.08	0.11	0.11	0.04	0.05	0.08	0.07	0.10	0.03	0.07
MgO	4.34	3.80	2.98	3.49	3.24	3.33	2.26	3.79	1.63	1.60	2.28	1.83	3.89	2.47	3.65
CaO	4.69	5.04	3.94	4.79	5.22	4.96	4.37	4.75	3.01	2.86	4.34	2.21	5.84	3.81	4.20
Na_2O	2.71	2.94	3.28	2.80	2.84	2.94	2.94	2.90	3.52	3.49	2.85	3.10	3.20	3.52	3.82
K_2O	2.22	2.59	2.75	2.35	2.14	2.37	3.36	3.15	3.76	4.02	3.64	4.31	2.80	2.94	2.98
P_2O_5	0.12	0.13	0.13	0.11	0.14	0.13	0.13	0.15	0.16	0.16	0.21	0.19	0.16	0.16	0.17
LOI	3.92	3.79	3.17	3.63	3.32	3.22	1.00	2.33	1.03	1.04	1.58	1.89	3.22	2.49	1.14
total	100.7	100.4	99.67	100.1	99.86	100.2	99.74	99.79	98.71	98.92	100.3	99.18	100.6	100.2	99.18
V	205	148	131	155	187	135	109	141	62	68	102	67	171	119	114
Cr	60.4	20.6	13.4	31.2	42.0	36.0	22.0	113	19.6	20.2	23.7	15.4	80.0	45.0	40.0
Co	20.5	13.3	13.5	16.5	16.0	13.0	12.0	17.4	6.8	4.6	9.8	6.9	20.0	13.0	12.0
Ni	12.1	7.67	6.17	9.18	12.6	14.1	11.5	25.4	8.49	7.52	8.32	5.97	15.6	14.2	18.4
Zn	92	66	46	60	85	55	51	67	10	19	32	43	110	35	68
Ga	14	17	16	20	13	17	18	16	20	21	19	22	14	14	13
Rb	87	81	64	72	78	63	146	139	181	189	136	187	123	64	101
Sr	230	287	290	189	207	256	228	381	260	270	356	278	281	260	272
Li	25	34	21	32	25	27	27	15	26	27	22	47	30	28	33
Ba	251	333	381	330	247	319	702	870	731	805	925	766	625	631	472
Pb	7.0	21	12	18	14	10	24	28	49	32	26	48	19	10	16
Y	25.4	18.1	18.7	22.6	20.1	17.7	22.3	22.5	17.7	18.9	18.5	14.9	23.8	20.6	20.5
Sc	23	24	20	23	21	18	19	21	16	17	20	18	29	22	19
Zr	94	94	111	107	85	117	166	152	136	129	150	96	135	170	149
Nb	6.95	8.07	9.14	8.69	7.81	8.20	12.9	13.9	16.6	17.2	14.9	15.8	9.10	12.2	10.3
Ta	0.58	0.62	0.80	0.80	0.60	0.68	1.23	1.42	2.14	2.28	1.58	1.96	0.78	1.10	0.87
Hf	2.5	2.5	3.0	3.0	2.2	3.0	4.1	4.0	3.7	3.6	4.0	2.8	3.3	4.1	3.6
Th	4.75	5.88	7.46	7.15	5.12	7.14	19.6	19.2	18.6	19.1	19.2	17.3	11.5	13.5	8.30
U	1.73	1.90	2.62	2.72	2.54	2.66	5.07	6.91	8.16	7.51	7.02	6.30	4.33	4.42	2.83
La	12.9	18.3	21.6	18.4	14.1	19.8	27.3	26.2	25.7	29.4	26.9	20.9	22.4	33.4	27.2
Ce	25.7	35.3	39.7	35.9	30.8	41.6	55.1	52.9	49.5	54.7	50.8	42.8	46.1	68.2	56.4
Pr	3.29	4.13	4.50	4.29	3.55	4.64	6.03	6.45	5.53	6.13	5.71	4.67	5.24	7.43	6.13
Nd	13.2	15.2	16.1	16.2	13.4	16.9	21.1	25.1	19.6	21.3	20.4	16.5	19.4	26.0	22.1
Sm	3.56	3.35	3.47	3.81	3.12	3.60	4.48	5.64	4.22	4.35	4.21	3.67	4.32	5.38	4.50

Table 1 (continued)

	CS 42	CS 56	CS 66	CS 88	CS 91	CS 69	CS 97	CS 22	CS 39	CS 53	CS 59	CS 89	CS 32	CS 54	CS 57
Eu	0.88	0.89	0.84	0.86	0.77	0.86	0.86	1.19	0.82	0.85	0.91	0.71	0.92	1.11	0.99
Gd	3.64	2.93	3.07	3.49	3.14	3.29	3.81	4.37	3.31	3.43	3.34	2.75	3.92	4.81	3.95
Tb	0.62	0.46	0.47	0.57	0.55	0.55	0.64	0.64	0.49	0.52	0.50	0.44	0.67	0.78	0.66
Dy	3.64	2.87	2.94	3.52	3.19	3.06	3.59	3.61	2.78	2.87	2.95	2.47	3.86	4.51	3.62
Ho	0.76	0.56	0.60	0.70	0.67	0.60	0.71	0.68	0.51	0.54	0.56	0.48	0.78	0.91	0.72
Er	2.26	1.67	1.73	2.08	1.91	1.84	2.15	1.90	1.47	1.53	1.63	1.35	2.23	2.63	2.05
Tm	0.32	0.24	0.25	0.30	0.30	0.29	0.33	0.28	0.21	0.21	0.23	0.20	0.35	0.41	0.32
Yb	2.31	1.69	1.87	2.12	1.99	1.88	2.26	2.00	1.50	1.59	1.71	1.41	2.28	2.61	2.17
Lu	0.34	0.26	0.30	0.32	0.29	0.30	0.35	0.30	0.23	0.24	0.28	0.23	0.36	0.41	0.33

For analytical details, see chapter Analytical techniques

0.87 to 0.63. The primitive mantle-normalized trace element patterns have a shape that is typical of volcanic rocks from subduction-related tectonic settings. They are enriched in the LILE (Large Ion Lithophile Elements), U, Th, Pb, LREE relative to HREE and are depleted in Nb, Ta, P and Ti (Fig. 5). Isotope compositions are presented in Table 2. Both, the initial $^{87}Sr/^{86}Sr$ and the initial $^{143}Nd/^{144}Nd$ isotope ratios (expressed as εNd) are variable ranging from 0.7085 to 0.7113 for $^{87}Sr/^{86}Sr$ and from – 2.0 to – 6.7 for εNd (Fig. 6). Initial Hf isotope compositions (expressed as εHf) vary from – 4.0 to + 2.5. $\delta^{18}O$ values range from + 6.5 ‰ to + 9.1 ‰. $^{206}Pb/^{204}Pb$, $^{207}Pb/^{204}Pb$ and $^{208}Pb/^{204}Pb$ isotope ratios range from 18.50 to 18.73, 15.59 to 15.66, and 38.30 to 38.75, respectively (Fig. 7).

Discussion

Fractional crystallization and continental crustal contamination

The crystal fractionation history of arc magmas involves fractionation of olivine, spinel, and clinopyroxene from high-Mg basalt to basaltic andesite. Further fractionation from basaltic andesite to andesite involves minor clinopyroxene, amphibole and minor plagioclase (Hürlimann et al. 2016). This sequence of fractionation steps is seen in decreasing FeO, MgO, CaO, Ni, Cr, and increasing K_2O, Rb, Hf, Zr, Th, U, Ta, Pb, Nb and Ba from high-Mg rocks towards the andesites (Figs. 2 and 3). Interestingly, Al_2O_3 first increase from high-Mg basalt to basaltic andesite. This feature can be interpreted as a sign of high-pressure fractional crystallization due to a lack of plagioclase fractionation. Further, Al_2O_3 then decreases towards the andesites–dacites implying plagioclase fractionation, compatible with the negative Eu anomaly seen in the REE pattern (Fig. 4). The decrease in TiO_2 together with the development of a negative Ti-anomaly in the multielement diagram (Fig. 5) implies fractionation of amphibole where Ti becomes compatible in amphibole (Hürlimann et al. 2016). Like in many continental arcs worldwide, rocks that represent primary magmas are absent among the suite investigated here and even the most mafic samples have low abundances of MgO, Ni and Cr suggesting that the parental magmas underwent significant crystal fractionation of likely olivine and pyroxene (Hürlimann et al. 2016). Since isotope compositions vary with elemental abundances (Fig. 8), these isotopic trends are interpreted as indicating assimilation of crustal material (AFC; DePaolo 1981) or sediment melt mediated source enrichment and subsequent partial melting of those sources. The correlation of LILE enrichment, K in particular, and radiogenic isotopic composition supports the inference that the K-rich character is, at least, in part related to continental crustal

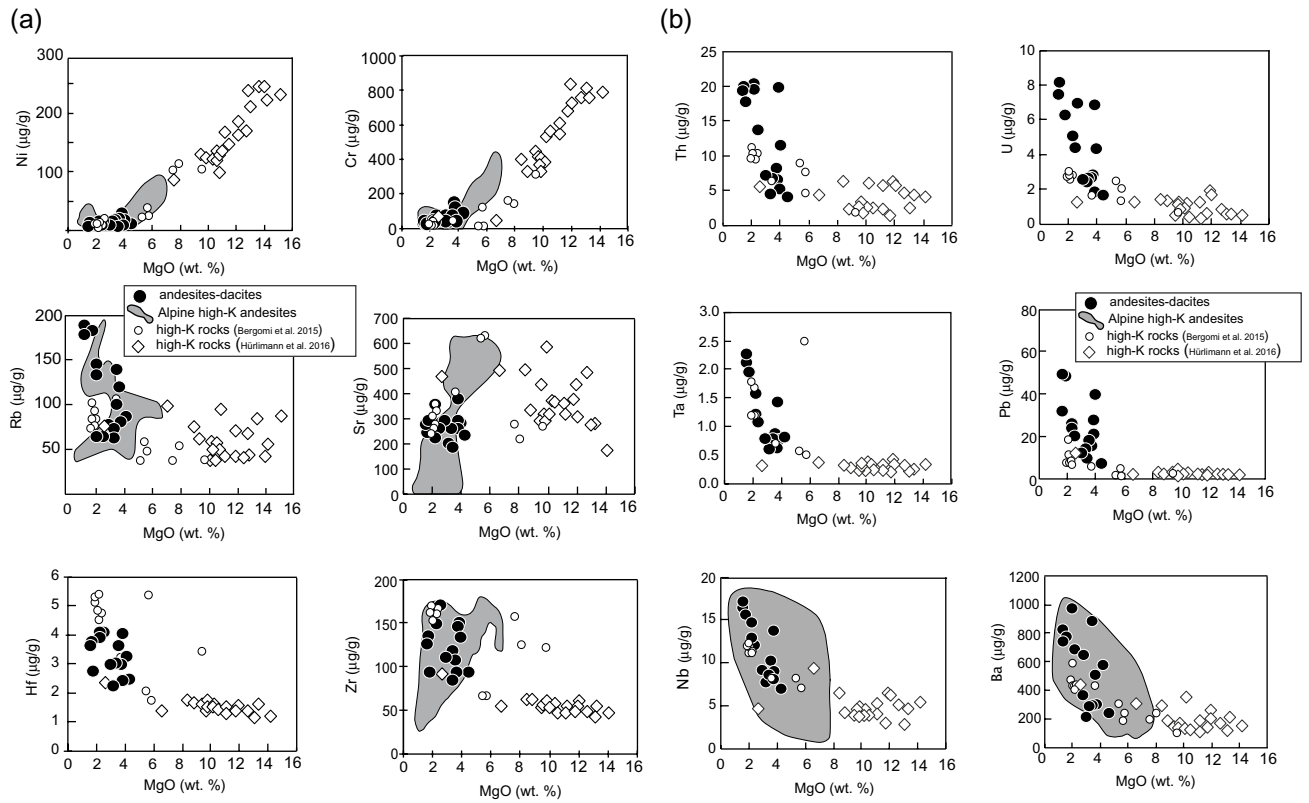

Fig. 3 Selected trace element diagrams of the andesites and dacites. Grey field denote data for other high-K andesites and dacites from the Alps according to Deutsch (1984), Beccaluva et al. (1979), Diethelm (1990), Gautschi and Montrasio (1978), Dal Piaz et al. (1979), (1988) and Ruffini et al. (1997). Reference data for mafic high-K rocks from Hürlimann et al (2016) and Bergomi et al. (2015) are shown for comparison

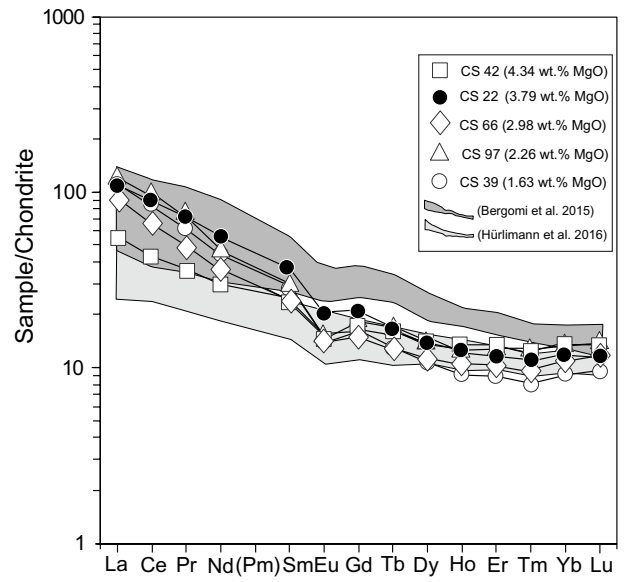

Fig. 4 Rare-earth element abundances of selected andesites and dacites. Normalization values from Palme et al. (2014). Reference data for mafic high-K rocks from Hürlimann et al. (2016) and Bergomi et al. (2015) are shown for comparison

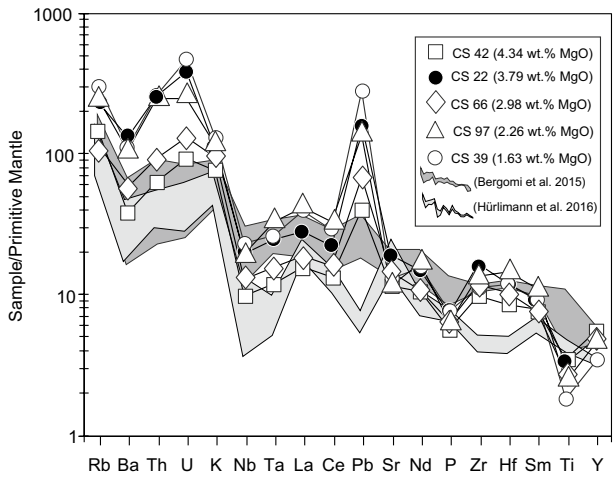

Fig. 5 Primitive mantle-normalized incompatible element patterns of selected andesites and dacites. Normalization values from Sun and McDonough (1989). Reference data for mafic high-K rocks from Hürlimann et al (2016) and Bergomi et al. (2015) are shown for comparison

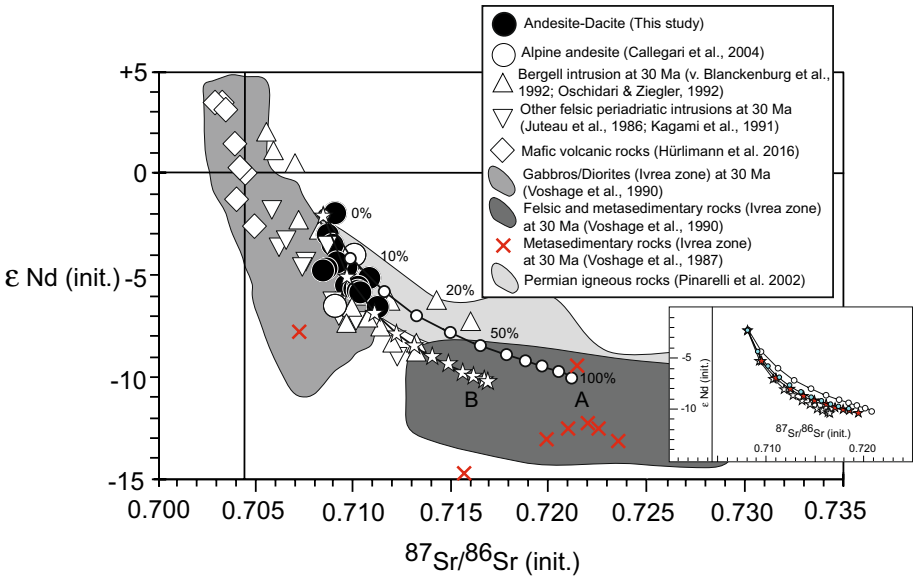

Fig. 6 εNd vs. $^{87}Sr/^{86}Sr$ diagram showing data for the andesites and dacites. Superimposed are possible calculated AFC curves. Calculation A uses the composition of a basement rock from Voshage et al. (1990) with 207 ppm Sr ($^{87}Sr/^{86}Sr$: 0.721) and 33 ppm Nd (εNd: – 10.3). The starting andesite has 250 ppm Sr ($^{87}Sr/^{86}Sr$: 0.708) and 15 ppm Nd (εNd: – 1.9) similar to the unevolved sample CS 56. Bulk Kd values were 1 for Sr and 0.8 for Nd with an *r* value (ratio of assimilation to fractionation) of 0.6. Calculation B uses a Hercynian granite (Pinarelli et al. 2002) with 293 ppm Sr ($^{87}Sr/^{86}Sr$: 0.71663) and 52.4 ppm Nd (εNd: – 10.7). Bulk Kd values and *r* value as in calculation A. AFC paths imply up to 20% assimilation of crustal material. Note that primitive mafic rocks (Hürlimann et al. 2016) also record some variation in Sr–Nd isotope composition that can also be explained by limited uptake of crustal material. Inset shows AFC calculation using the EC-AFC model of Spera and Bohrson (2001) with parameters given in Table A5 (Kagami et al. 1991)

contamination that caused an increase in K_2O coupled with an increase in $^{206}Pb/^{204}Pb$ and a decrease in εHf and εNd values (Fig. 9). Metasedimentary rocks from the Alps are too unradiogenic to serve as a source (eNd: – 11 to – 9, Henry et al. 1997) but may be potential contaminants. A lack of data precludes a more detailed evaluation in this case.

In a plot of εNd vs. $^{87}Sr/^{86}Sr$ (Fig. 7), the samples define part of a curved array that is consistent with simple two-component mixing between a hypothetical mantle component and a lower crustal component. Granulite-facies metasedimentary rocks from the alpine basement (Voshage et al. 1990) have radiogenic Sr and less radiogenic Nd isotope compositions and up to 20% assimilation of such rocks by the most primitive andesite may explain the isotope composition of the most evolved andesites and dacites. Although some of these Hercynian gneisses and metasediments have undergone extensive partial melting (Schnetger 1994) and may thus not represent fertile lithologies, they represent a crustal endmember with radiogenic Sr and unradiogenic Nd isotope signatures. Additional presumably more fertile potential contaminants are Permian granitoids that intruded the area (Pinnarelli et al. 2002). In addition, the andesites and dacites have a relatively large range in $^{207}Pb/^{204}Pb$, $^{208}Pb/^{204}Pb$ and $^{206}Pb/^{204}Pb$ ratios (Fig. 7) supporting that assimilation of ancient continental crust played a role in the evolution of these samples. In Fig. 7, the Pb isotope composition of Hercynian lower crustal mafic, felsic and metasedimentary rocks from the Ivrea zone (Southern Alps), some Alpine upper crustal granites and Permian granites from the Southern Alps as potential assimilants are plotted. Lead isotope data from lower crustal rocks from the southern Alps are limited (Cumming et al. 1987) but alpine granites and Permian granites from the southern Alps have distinctly more radiogenic Pb isotope compositions, and considering Pb isotopes alone, the andesites and dacites may be differentiated mantle wedge derived magmas that underwent substantial assimilation of upper crustal material with a Pb isotope signature similar to that of the Alpine granites or the Permian granites (Fig. 7). Potential mantle-derived subducted material (Cannaò et al. 2015; McCarthy and Müntener 2019) show a large range in Pb isotopes with nearly complete overlap with the andesites–dacites studied here making an evaluation of the significance of such material in the genesis of the andesites–dacites impossible. It is, therefore, assumed that the Pb isotope signature of the andesites and dacites reflects a combination of crustal assimilation and source features, where fluids or partial melts from subducted material (upper mantle rocks, mantle-derived igneous rocks, and metasediments) imprinted an upper continental crustal-dominated Pb isotope signature to the mantle wedge prior to melting.

Table 2 Rb–Sr, Sm–Nd, Lu–Hf. Pb and O isotope data for andesites–dacites from the Alps (Italy)

	CS 42	CS 56	CS 66	CS 88	CS 91	CS 69	CS 97	CS 22	CS 39	CS 53	CS 59	CS 89	CS 32	CS 54	CS 57
$^{143}Nd/^{144}Nd$(m)	0.512526	0.512373	0.512388	0.512436	0.512463	0.512381	0.512335	0.512306	0.512320	0.512317	0.512317	0.512328	0.512383	0.512346	0.512281
$^{143}Nd/^{144}Nd$(i)	0.512497	0.512348	0.512364	0.512409	0.512435	0.512356	0.512310	0.512278	0.512295	0.512293	0.512293	0.512304	0.512357	0.512322	0.512257
εNd(i)	−2.0	−4.9	−4.6	−3.7	−3.2	−4.8	−5.6	−6.3	−5.9	−6.0	−6.0	−5.8	−4.7	−5.4	−6.7
$^{147}Sm/^{144}Nd$	0.149	0.129	0.124	0.137	0.140	0.128	0.128	0.143	0.127	0.121	0.121	0.121	0.134	0.125	0.123
Sm (ppm)	3.46	3.32	3.18	3.59	3.12	3.60	4.48	4.46	3.91	4.10	4.12	3.64	4.32	5.38	4.50
Nd (ppm)	14.1	15.6	15.5	15.9	13.4	16.9	21.1	18.9	18.6	20.4	20.6	18.2	19.4	26.0	22.1
TDM	1.28	1.25	1.17	1.26	1.26	1.23	1.30	1.60	1.31	1.24	1.24	1.22	1.31	1.24	1.31
$^{87}Sr/^{86}Sr$(m)	0.709672	0.708933	0.709621	0.709482	0.709168	0.708989	0.710612	0.710607	0.711114	0.711238	0.710699	0.711220	0.710150	0.711073	0.711768
$^{87}Sr/^{86}Sr$(i)	0.7092	0.7085	0.7093	0.7090	0.7087	0.7087	0.7098	0.7102	0.7103	0.7104	0.7102	0.7103	0.7096	0.7108	0.7113
$^{87}Rb/^{86}Sr$	1.163	0.916	0.767	1.112	1.091	0.712	1.854	1.0346	1.9199	1.9975	1.1609	2.2494	1.2670	0.7125	1.0748
Rb (ppm)	82.7	80.7	67.8	77.9	78.0	63.0	146	139.9	178.7	188.2	137.8	181.3	123.0	64.0	101.0
Sr (ppm)	205.8	254.8	256.0	197.4	207.0	256.0	228.0	391.26	268.71	266.22	349.13	233.25	281.0	260.0	272.0
δ^8O (‰)	6.9	8.0	7.4	6.5	8.5	9.1	n.d.	7.7	7.9	8.6	7.8	8.3	n.d.	6.7	n.d.
$^{176}Lu/^{177}Hf$	0.0177	0.0195	0.0119	0.0137	0.0164	0.0171	0.0139	0.01055	0.01085	0.009143	0.01196	0.01052	0.01399	0.01366	0.01523
$^{176}Hf/^{177}Hf$(m)	0.282847	0.282731	0.282720	0.282774	0.282831	0.282780	0.282739	0.282663	0.282659	0.282700	0.282664	0.282659	0.282773	0.282728	0.282691
$^{176}Hf/^{177}Hf$(i)	0.282837	0.282720	0.282713	0.282766	0.282821	0.282771	0.282731	0.282657	0.282653	0.282695	0.282657	0.282653	0.282765	0.282720	0.282682
ε Hf (i)	2.5	−1.6	−1.9	0.0	2.0	0.2	−1.2	−3.8	−4.0	−2.5	−3.8	−4.0	−0.1	−1.6	−3.0
Hf (MC-ICP-MS)	2.683	1.855	3.087	3.191	2.530	1.947	2.913	3.881	2.947	3.760	3.012	3.132	3.218	3.550	2.429
Lu (MC-ICP-MS)	0.346	0.264	0.268	0.318	0.302	0.243	0.296	0.298	0.233	0.251	0.263	0.240	0.328	0.354	0.270
$^{206}Pb/^{204}Pb$	18.50	18.63	18.52	18.54	18.60	18.59	18.56	18.59	18.72	18.64	18.63	18.66	18.68	18.50	18.58
$^{207}Pb/^{204}Pb$	15.60	15.61	15.60	15.59	15.63	15.60	15.60	15.61	15.65	15.60	15.61	15.61	15.63	15.60	15.62
$^{208}Pb/^{204}Pb$	38.30	38.45	38.34	38.33	38.47	38.36	38.39	38.51	38.66	38.46	38.51	38.51	38.67	38.34	38.45

Rb, Sr, Sm and Nd were measured by N-TIMS and Lu and Hf were measured by MC-ICP-MS. Analytical in-run errors are typically 0.000015 or less. Calculation of εNd values is relative to CHUR according to Jacobsen and Wasserburg (1980). Nd model age (TDM) calculation is according to Michard et al. (1985). Pb isotope ratios were recalculated using U, Th and Pb abundances from Table 2 assuming an age of 30 Ma. For analytical details, see text. (m): measured. (i): initial

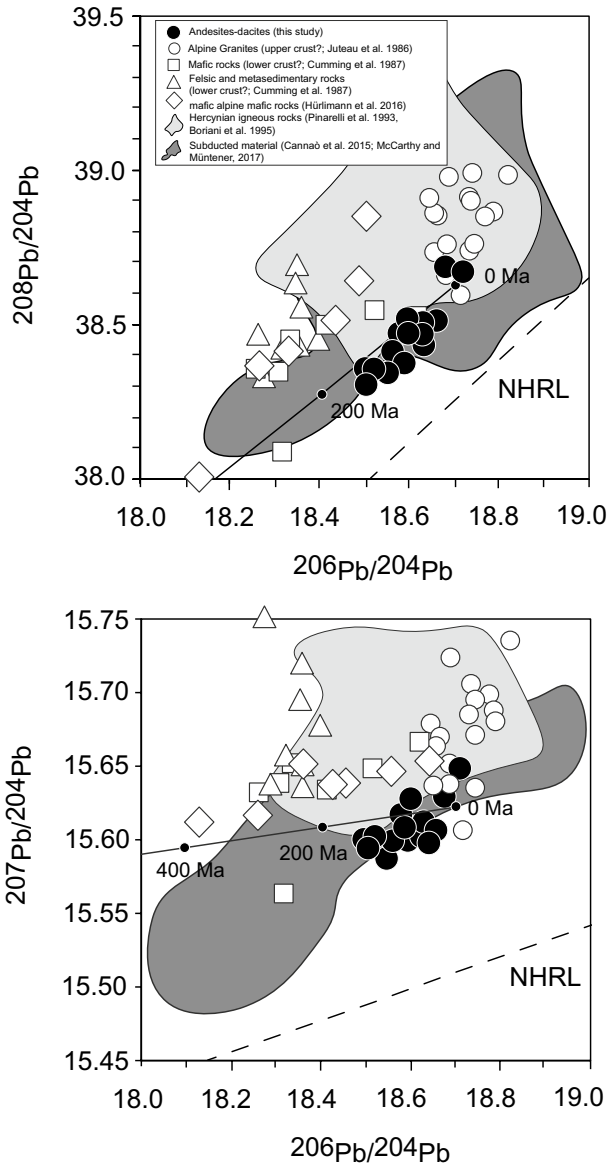

Fig. 7 Plot of **a** $^{208}Pb/^{204}Pb$ and **b** $^{207}Pb/^{204}Pb$ versus $^{206}Pb/^{204}Pb$ isotope ratios for the andesites and dacites. Also shown are reference data for alpine granites from Juteau et al. (1986), mafic, felsic and metasedimentary rocks from Cummings et al. (1987) and Permian igneous rocks (light grey-shaded field) from Pinarelli et al. (1993) and Boriani et al. (1995). The dark grey-shaded fields show data from Jurassic mafic rocks that may potentially represent subducted mafic material. Note that mafic and felsic lower crustal rocks are too unradiogenic in $^{206}Pb/^{204}Pb$ to serve as possible contaminants and Permian igneous rocks, although most of them are slightly too radiogenic, are more likely candidates for crustal assimilation, at least with respect to the Pb isotope composition

The question then arises whether assimilation of crustal rocks occurred as bulk assimilation (DePaolo 1981) or selective assimilation (Glazner 2007). In contrast to bulk assimilation where the entire lower crustal rocks are assimilated, selective assimilation is a process where partial melts consisting of mineral assemblages with a low melting point (feldspars, mica) from the lower crustal rocks are incorporated into the rising magma. The size of the magma chamber(s) that fed the andesites–dacites is not known but their fairly evolved nature suggests that bulk assimilation is unlikely. The lower crust in the southern Alps consists of high-grade metamorphic rocks (kinzigites, stronalites) in which the granulite-facies stronalites are melt-depleted (Schnetger 1994) and may thus represent non-fertile contaminants. More fertile rocks are the amphibolite-facies kinzigites and the Permian granites that intruded the area. Thus, incorporation of partial melts consisting of plagioclase, K-feldspar and biotite from the lower crust seems more reasonable. To constrain the thermal effects of a rising andesite magma incorporating low-melting components from lower crustal metasedimentary or igneous sources, we performed several calculations using the EC-AFC software package (Spera and Bohrson 2001). The results are shown in the inset to Fig. 6 and the EC-AFC parameters used are given in Table A5. It is important to note that we want to show the evolution within the andesite–dacites and not the evolution from more mafic high-K rocks (i.e., Hürlimann et al. 2016) towards the andesites. It is thus not surprising that the results using EC-AFC calculation are broadly similar to those derived by common AFC calculations (i.e., DePaolo 1981). Estimated degrees of assimilation are about 20% using both, a non-depleted kinzingite (Voshage et al. 1987) from the Alpine basement and a Permian granite (Pinarelli et al. 2002) that intruded the area (Fig. 7).

The Nb/Ta ratio is also strongly correlated with indices of fractional crystallization such as SiO_2 and K_2O (Fig. 8) in which the most fractionated rocks have the lowest Nb/Ta. This implies that during fractionation, minerals with high Nb/Ta were fractionated. These minerals were likely amphibole and biotite (Müntener et al. 2018) which are important phenocrysts phases in the andesites. In addition, Nb/Ta is also correlated with εHf suggesting some modification of this ratio during AFC processes. This view is compatible with the Nb/Ta of lower crustal rocks which is substantially lower than upper crustal or MORB estimates (Nb/Ta: 8.3; Rudnick and Gao 2004). A full set of HFSE on felsic and mafic lower crust from the alpine basement is not available, therefore, precluding a more detailed evaluation using local endmembers.

In Hf–Nd isotope space, the samples deviate from the crustal array (Vervoort and Patchett 1996), a line which marks the co-variation of both isotope systems during magmatic differentiation and crustal evolution (Fig. 9). Assimilation of bulk sediment that diverts from the array through the zircon effect is expected to show a deviation towards radiogenic Nd at unradiogenic Hf (Woodhead et al. 2017), however, the opposite of what is observed. This Hf–Nd isotope decoupling hence implies interaction of an inferred

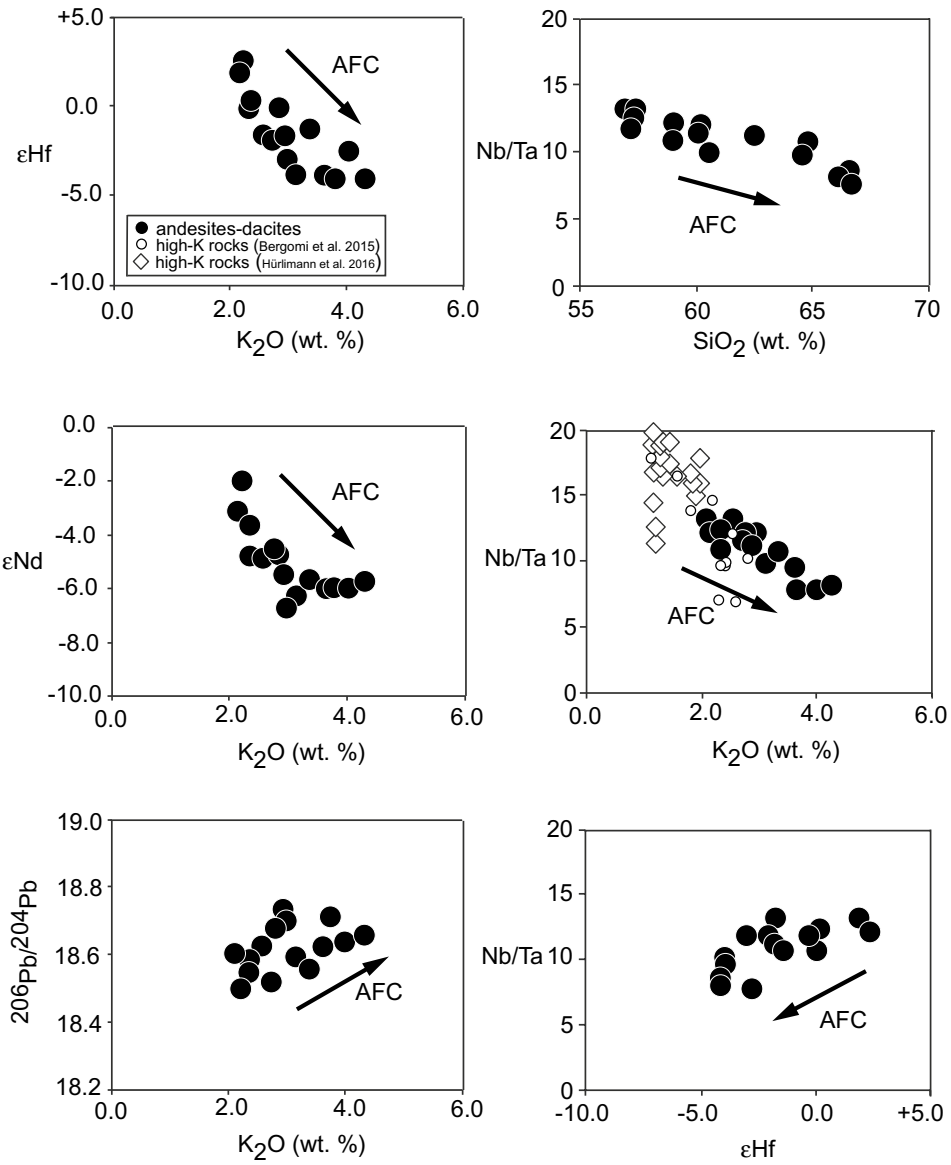

Fig. 8 Diagram of εHf, εNd, $^{206}Pb/^{204}Pb$ vs. K_2O and Nb/Ta vs. SiO_2, K_2O and εHf. Correlations among these parameters indicate assimilation of crustal material. Note that mafic high-K rocks from Hürlimann et al. (2016) und Bergomi et al. (2015) plot along the same AFC path in Nb/Ta vs. K_2O. For more details, see text

primary magma with a reservoir that shows radiogenic Hf at unradiogenic Nd, a feature typical for aged garnet-bearing rocks. Assimilation of Hercynian garnet-bearing lithologies of the lowermost crust would create the observed deviation, and agrees with the correlation observed for Nd–Sr isotope compositions (Fig. 6). Oxygen isotope constraints support a crustal influence during magma differentiation, as oxygen isotopes of the andesites and dacites (6.5–9.1 ‰) are heavier than average MORB (5.4–6.1 ‰; Ito et al. 1987; Eiler 2001). The lack of correlation between oxygen isotopes and radiogenic isotopes as well as trace elements, however, implies that fluid–rock interaction along with crustal contamination likely modified the primary oxygen isotope composition. In conclusion, the most feasible scenario to explain the geochemical features of the andesites and dacites is wall-rock assimilation possibly in the lower crust where heat fluxes are high. Such a scenario fails to explain the high amounts of LILE and K as well as the radiogenic Pb isotope signatures observed in the samples, which require additional assimilation of more evolved silicic upper crustal rocks, or need to be source features that have been imprinted to the depleted mantle wedge by fluid addition or sediment melt from the slab prior to melting.

The results from this study support previous studies on the generation of arc-derived magmatic rocks that also provided clear evidence for the involvement of continental crustal material during their evolution (Davidson et al. 1990; Hildreth and Moorbath 1988; Davidson and Harmon 1989; Rogers and Hawkesworth 1989; Ellam and Harmon 1990; Thirlwall et al. 1996 among many others). Whereas some studies concluded that these crustal signatures are pre-melting features of the mantle wedge caused by fluid and

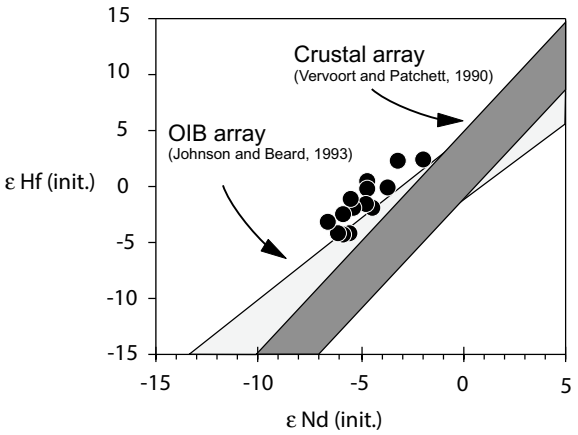

Fig. 9 Plot of initial εHf vs. initial εNd for the andesites and dacites. Also shown are arrays for continental crust (Vervoort and Patchett 1996) and OIB (Johnson and Beard 1993). The deviation towards radiogenic Hf imply involvement of an ancient high Lu/Hf endmember, most likely garnet-bearing lower crust

sediment or sediment melt addition from the down-going slab (e.g., Keppler 1996; Elliott et al. 1997; Elliott 2003; Kelemen et al. 2004; Chen et al. 2021), other studies provided evidence that these crustal signatures reflect differentiation processes within different levels of the arc crust (e.g., Jagoutz 2014; Jagoutz and Kelemen 2015; Ducea and Saleeby 2015; Tang et al. 2019; Pfänder et al. 2021), or are a combination of both. It is evident, that post-melting assimilation and fractional crystallization (AFC) may also modify the geochemical signatures of arc magmas.

The role of slab-derived components and sediment subduction

Some of the K-rich character may be attributed to combined fractional crystallization–assimilation processes consistent with the correlation between radiogenic isotope compositions and K_2O (Fig. 8). However, average continental crust has only 1.8 wt. % K_2O (Rudnick and Gao 2004) and, therefore, assimilation of specific K-rich lithologies (glimmerites, metapelites, K-rich granites) is required. Alternatively, processes other than fractional crystallization–assimilation or specific sources may have contributed to the K-rich nature. An extrapolation back to c. 50 wt. % SiO_2 (Fig. 2) suggests that the hypothetical parental melts also had a high-K character (1.5–2.0 wt. %; Hürlimann et al. 2016) and it is proposed that the infiltration of slab-derived fluids or melts from subducted pelagic sediments produced substantial chemical enrichments in the mantle wedge and hence in the melts derived from it.

Fluid phases produced by slab dehydration effectively concentrate Ba, Pb, Sr and other LILE among further elements such as U (Myers and Marsh 1987; Ben Othman et al. 1989; Kessel et al. 2005). Therefore, incompatible trace element ratios involving Ba relative to fluid-immobile trace elements of similar incompatibility (Nb, La, and Zr) should be high as long as a slab-derived fluid phase is involved (Fig. 10; McCulloch and Perfit 1981; Tatsumi et al. 1986). Since average continental crust has low Ba/La (22.8), Ba/Nb (57) and Ba/Zr (3.5) ratios (Rudnick and Gao 2004), the

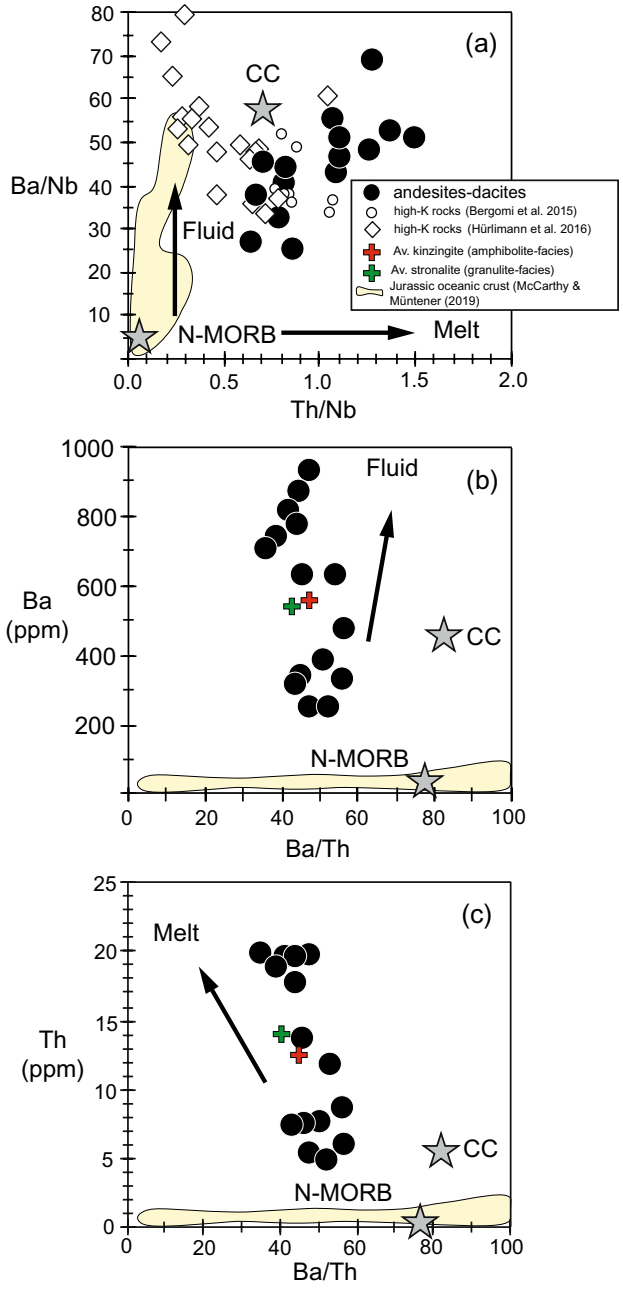

Fig. 10 **a** Ba/Nb vs. Th/Nb, **b** Ba vs. Ba/Th and **c** Th vs. Ba/Th variation showing the presence of fluid (high Ba, high Ba/Nb) and melt (high Th/Nb, high Th) in the evolution of the andesites and dacites. Compositions of continental crust (CC) and MORB are taken from Rudnick and Gao (2004) and Gale et al. (2013), respectively

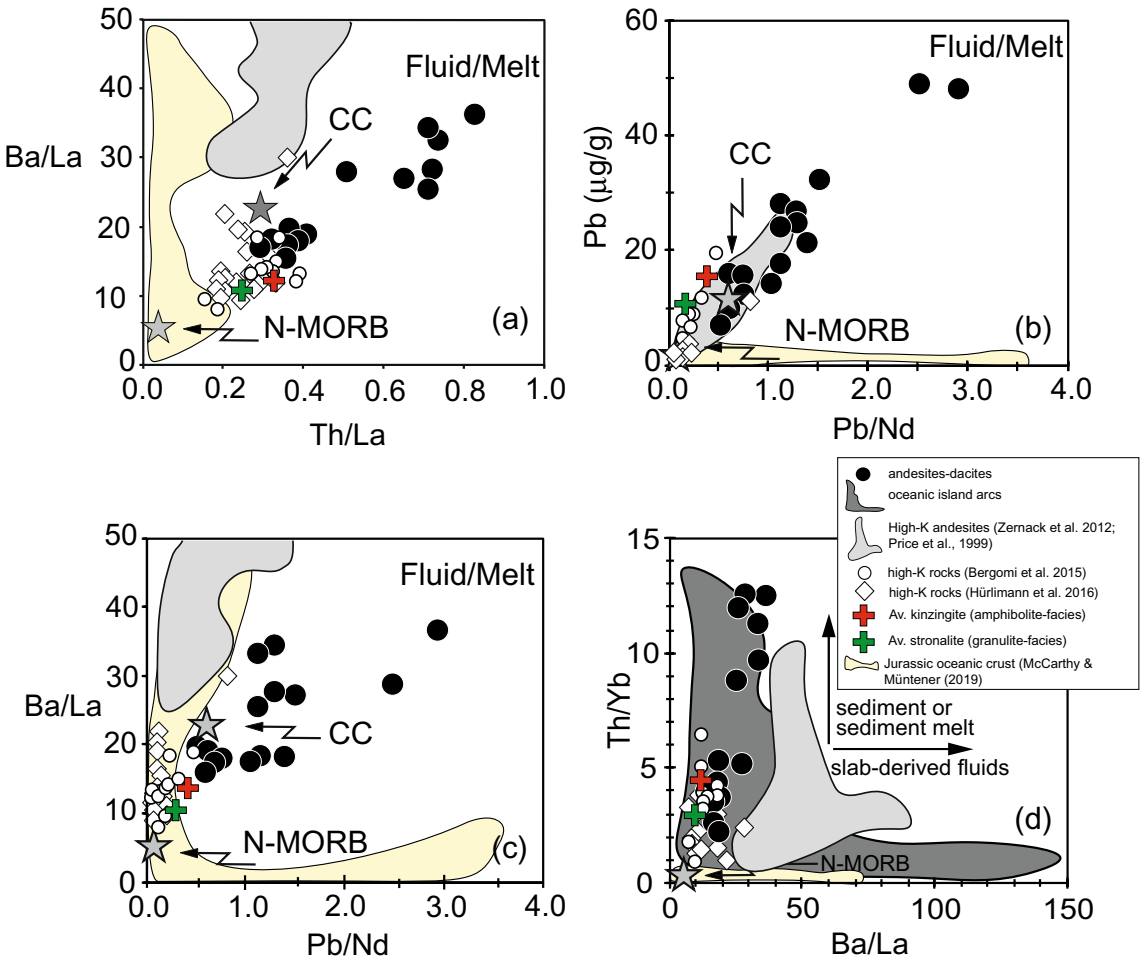

Fig. 11 Plot of **a** Ba/La vs. Th/La, **b** Pb (in µg) vs. Pb/Nd, **c** Ba /La vs. Pb/Nd and **d** Th/Yb vs. Ba/La for the andesites and dacites to illustrate the effects of fluid/melt interaction. Compositions of continental crust (CC) and MORB are taken from Rudnick and Gao (2004) and Gale et al. (2013), respectively

variable and in part higher ratios of these elements observed in the andesites–dacites (Ba/La: 16–37, Ba/Nb: 32–69 and Ba/Zr: 2.7–8.0) are unlikely to result from crustal contamination alone and follow more likely from fluid infiltration from the slab to the mantle wedge.

All samples have high Pb abundances which are substantially higher than in continental arc andesites which on average have 4–8 ppm Pb (Kelemen et al. 2004). Lead is an aqueous fluid-mobile element (Brenan et al. 1995) and when plotted against Nd because of their similar melt-peridotite partition coefficients and because Nd is less fluid-mobile than Pb, linear relationships between Pb abundances and Pb/Nd ratios are expected for rock series from aqueous fluid-enriched sources, a feature observed for the andesites and dacites (Fig. 11). Moreover, the samples with high Ba/La ratios have also high Pb/Nd ratios further strengthening the argument that an aqueous fluid was involved in magma genesis, along with sediment-derived melts. It is noteworthy that the latter should also have Pb/Nd ratios ≥ 1 (Münker 2000), which thus may have also contributed to the samples with Pb/Nd ≥ 1, compatible with the Ba/Nb–Th/Nb constraints. Other high-K andesites that also show high Ba/Nb and Th/Nb ratios (Price et al. 1999; Zernack et al. 2012) show low Ce/Pb and low-Nb/U ratios (Zernack et al. 2012: Ce/Pb < 8, Nb/U < 10; Price et al. 1999: Ce/Pb < 6, Nb/U < 10) that are commonly interpreted to indicate the presence of a fluid that was derived from subducted crustal sediments. (Ben Othman et al. 1989; Stern et al. 1993; Klein and Karsten 1996; Jackson et al. 2007). Similarly, Miller et al. (1994) have shown that low Ce/Pb in arc lavas are not generated through common melting processes but require the enrichment of Pb in the sources through incorporation of a sedimentary component in the presence of a fluid phase extracted from the subducted slab (MORB source). For the andesites and dacites from this study, Nb, U, Ce, and Pb increase with decreasing MgO (Fig. 3). Nb/U decreases with increasing Nb and U; the same is observed for Ce/Pb vs. Pb (Fig. 12) and Ce, although Ce is somewhat more scattered. More importantly,

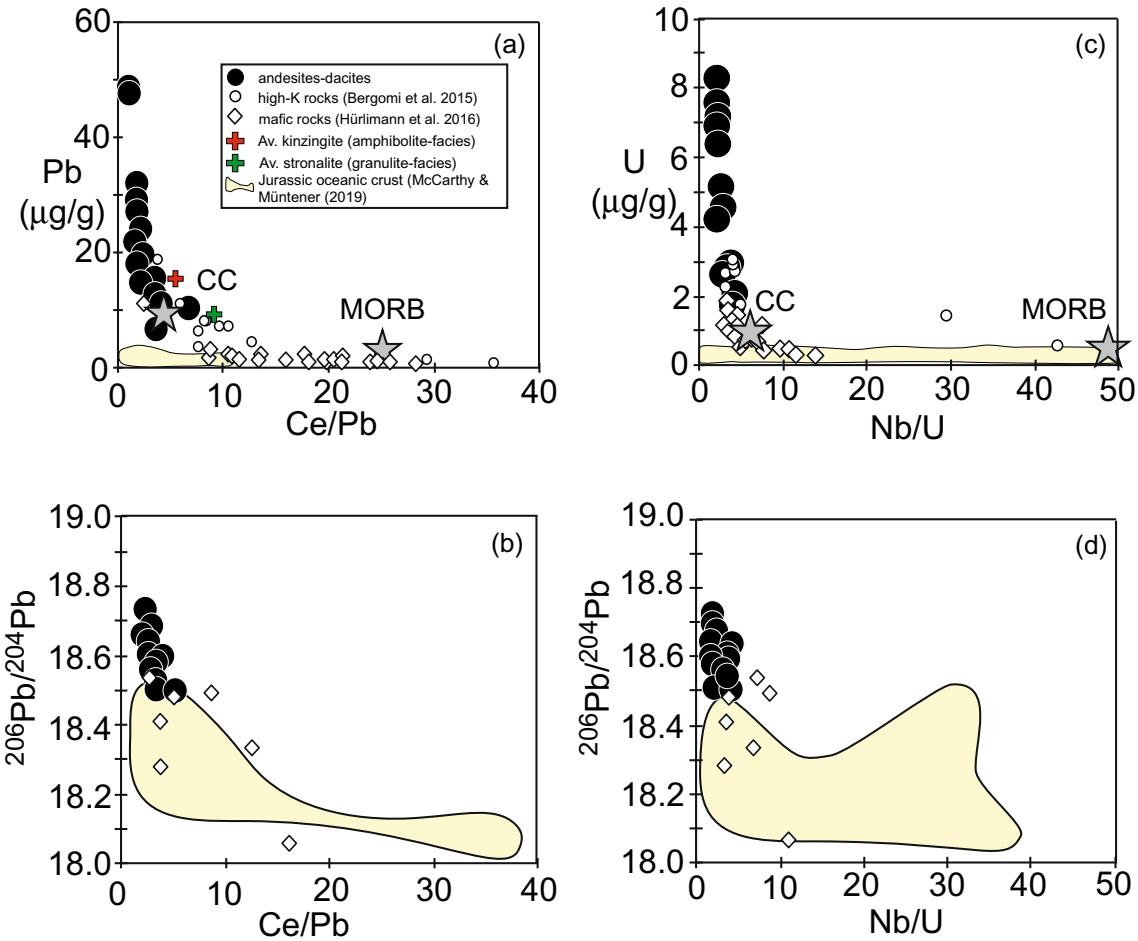

Fig. 12 Plot of Ce/Pb vs Pb, $^{206}Pb/^{204}Pb$ and Nb/U vs U and $^{206}Pb/^{204}Pb$

however, Ce/Pb (and Nb/U) ratios decrease with increasing $^{206}Pb/^{204}Pb$ (Fig. 12). In addition, Δ7/4 (+8.8 to +12.7) and Δ 8/4 (+38 to +39) values (Δ 7/4 and Δ 8/4 after Hart 1984; not shown in detail here) reveal an excess of radiogenic Pb with values that are similar to GLOSS estimates (GLObal Subducting Sediment; Plank and Langmuir 1998; Jackson et al. 2007). These features are consistent with the addition of a fluid phase with high Pb contents and a continental crustal-like Pb isotope signal to the mantle wedge, where the source of the fluid was most likely dehydrating subducting sediment. It is, however, not possible to distinguish clearly between a sedimentary component from the subducting slab and a lower crust-derived metasedimentary component.

Ba/Nb and Th/Nb are correlated among the andesites–dacites (Fig. 10). Thorium is considered to be a mostly fluid-immobile element that is strongly depleted in the residual mantle. However, Rustioni et al. (2021) observed some fluid mobility of Th at high salinity at 4 GPa and at low salinity at 6 GPa. This study does not provide Cl data to test this hypothesis and pressures of 4–6 GPa are potentially too high to be relevant for the generation of the andesites studied here. Elevated Th contents in arc-related magmas are, therefore, commonly explained by sediment or sediment melt addition from the down-going slab to the mantle wedge (e.g., Class et al. 2000; Woodhead et al. 2001). Ba is a hydrous fluid-sensitive trace element; hence, the positive correlation between Ba/Nb and Th/Nb implies the presence of hydrous fluid and sediment- or sediment melt in the source of the andesites–dacites. Ba/Th ratios are a proxy to estimate the fluid to sediment/sediment melt ratio of the fluxing component. The andesites–dacites from this study have low Ba/Th ratios between ~ 40 and 60 that are unrelated to Ba or Th contents (Fig. 10). Ba abundances (247–952 ppm) are similar but Th abundances (4.75–19.6 ppm) are higher relative to other high-K suites (Price et al. 1999: Ba/Th > 100 with Ba: 800–1200 ppm and Th < 10 ppm; Zernack et al. 2012: Ba/Th > 120 with Ba: 300–700 ppm and Th: < 7 ppm). This suggests a greater contribution of sediment or sediment-derived melt relative to aqueous fluid during mantle metasomatism in the case of alpine subduction. To further constrain the effect of addition of sediment or sediment melt, we evaluated the Th/Yb vs. Ba/La systematics (Fig. 11, Woodhead et al.

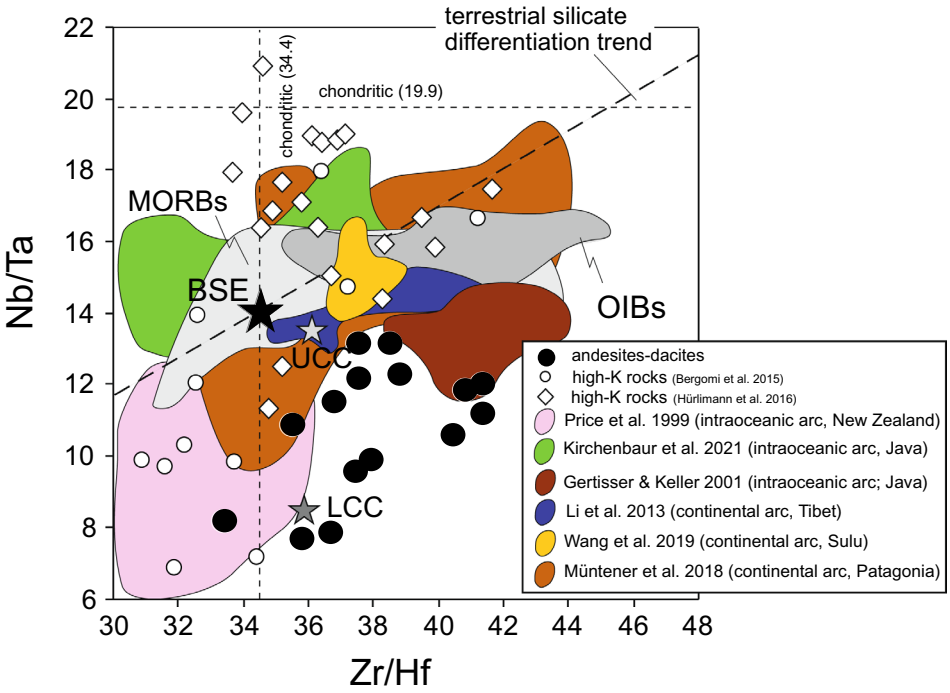

Fig. 13 Plot of Nb/Ta vs. Zr/Hf for the andesites–dacites. Figure taken and slightly modified from Pfänder et al. (2007). *BSE* Bulk Silicate Earth, *UCC* Upper Continental Crust and *LCC* Lower Continental Crust from Rudnick and Gao (2004); *MORB* Mid Ocean Ridge Basalt, *OIB* Ocean Island Basalt. Reference fields for various intra-oceanic and continental arcs are shown as well as reference data of high-K mafic rocks from Hürlimann et al. (2016) and Bergomi et al (2015). Note that both data sets show a trend towards low Nb/Ta similar to the andesites–dacites studied here. The trend can be interpreted as a result of combined AFC processes involving fractionation of amphibole and biotite (Müntener et al. (2018) combined with uptake of low- Nb/Ta lower crustal rocks (Gertisser and Keller 2003; Kirchenbaur et al. 2022)

2001). Figure 11 shows that the andesites–dacites exhibit a large variation in Th/Yb at low Ba/La which suggests that addition of sediment or sediment melt strongly contributed to the trace element variation in the andesites–dacites.

In conclusion, the trace element composition and Pb isotope composition of the andesites and dacites favor the addition of metasomatizing fluids and sediment-derived melts to the mantle wedge, with a dominance of the latter. Both components have been derived from dehydrating subducted sediments or hydrous sediment melts and possibly oceanic crust. To further constrain the significance of oceanic crust, we show data from Jurassic oceanic crust from the Alps (McCarthy and Müntener 2019) in Figs. 10, 11 and 12. The data show that this type of oceanic crust likely played only a minor role in the generation of the andesites–dacites studied here. The involvement of a sediment-derived melt requires comparatively high slab temperatures above the solidus of water-saturated metapelites (> 640 °C at pressures > 2 GPa; Mann and Schmitt 2015). Although such a model best explains the observed geochemical features and in particular the high-K contents, it is emphasized that the elemental and isotopic signals might be in part compromised by post-melting AFC processes within the crust.

Source constraints and intra-crustal differentiation deduced from HFSE systematics

High field strength elements (HFSE) are not transferred significantly to the mantle wedge during slab dehydration because of their low mobility in aqueous fluids (McCulloch and Gamble 1991; Brenan et al. 1995; Keppler 1996; Audétat and Keppler 2005; Antignano and Manning 2008). Therefore, concentrations and ratios of HFSE are insensitive to slab dehydration and mantle wedge metasomatism and mostly constrain the background composition of the mantle wedge (McCulloch and Gamble 1991; Woodhead et al. 1993; Elliott et al. 1997). Depleted HFSE contents relative to similarly incompatible trace elements and low-Nb/Ta and Zr/Hf ratios in arc volcanic rocks have been interpreted as reflecting remelting of a refractory mantle wedge that has been previously enriched in all but the HFSE by metasomatizing fluids, where the HFSE are retained and in part fractionated by residual Fe–Ti phases (mostly rutile) in the slab (the wedge depletion model of Plank and White 1995). The most primitive andesites from this study have low-Nb/Ta ratios of 11.7–13.0, which are lower than MORB estimates (Fig. 13) but not low abundances of HFSE. On the

other hand, Zr/Hf ratios cover the range observed in MORB (Fig. 13) and, therefore, the derivation of the parental magmas of the andesites–dacites from a common mantle peridotite that was depleted by a previous melting event seems not a viable process. This view is consistent with the inferred addition of sediment-derived melt and the negative correlation of Nb/Ta vs. Nb, which is the opposite of what is observed in arc rocks that result from remelting of depleted sources (Münker 1998).

Nb/Ta ratios in medium- to high-K subduction-related basalts and andesites are variable and can range from superchondritic (> 19.9) to subchondritic values as low as ~ 6 (Stolz et al. 1996; Münker 1998; Münker et al. 2004; Fig. 13). The subchrondritic values have been either explained by preferential retention of Nb in rutile (Münker 1998) or by shallow melting in the presence of residual amphibole with high Nb/Ta (König and Schuth 2011). Independent of the primary cause of low Nb/Ta in arc-related primary magmas, the negative correlation of Nb/Ta with SiO_2 observed in the andesites and dacites suggests post-melting fractionation of Nb and Ta, likely in the course of intra-crustal differentiation due to assimilation of low-Nb/Ta lower crustal rocks (Figs. 8 and 13). Nb, Ta, Zr and Hf concentrations from a coherent set of samples from the Ivrea Zone of the Alps, which were, based on isotope constraints, considered as potential assimilants (Fig. 6) are not available. However, a combination of trace element contents reported by Bea and Monteiro (1999) who do not report Hf concentrations and Schnetger (1994) who do not report Nb concentrations indicate Nb/Ta ratios between 11 and 18 and Zr/Hf ratios of ~ 43 for lower crustal rocks from the Alps. However, due to a lack of appropriate data a more compelling modeling is precluded. Despite the fact that crustal assimilation and magma mixing are considered to be fundamental in the generation or arc magmas (Grove et al. 1983), more recent studies emphasize the role of intra-crustal magma differentiation from basaltic to andesitic and dacitic magmas that are mainly controlled by crystal-liquid segregation (Jagoutz et al. 2009; Lee and Bachmann 2014; Tang et al. 2019; Pfänder et al. 2021). In these models, the trace element signatures of residual magmas depend on the crystallizing assemblages and relevant partition coefficients. The fractionation of ol + cpx + plag has limited effects on Nb/Ta due to the highly incompatible behavior of both elements (Adam and Green 2006), whereas the fractionation of amphibole with low Mg# (less than 70) can impart a lower Nb/Ta ratio to the coexisting melt (Foley et al. 2002; Müntener et al. 2018). Thus, fractionation of amphibole which are phenocrysts in the andesites may have in part contributed to the low Nb/Ta. Müntener et al. (2018) have also shown that fractionation of amphibole alone is not capable of decreasing Nb/Ta ratios significantly and another major mineral phase such as biotite is needed. Since biotite is an additional important mineral phase in the andesites, we concur with Müntener et al. (2018) that additional fractionation of biotite also contributed to the low Nb/Ta of the andesites–dacites. The described features, therefore, provide strong evidence that the andesites and dacites evolved by intra-crustal crystal–liquid differentiation, likely accompanied by assimilation of pre-existing Hercynian lower continental crust.

Conclusions and towards an evolutionary model for arc-related volcanism in the Alps

It is well known that subduction-related magmas originate in the mantle wedge above a subduction zone (e.g., Grove and Kinzler 1986; Crawford et al. 1987; Hawkesworth et al. 1991; McCulloch and Gamble 1991; Tatsumi and Eggins 1995 among many others). Dehydration reactions occurring in the lithosphere of the subducting plate release fluids and melts and interaction with the overlying mantle wedge generate primitive high-Mg basaltic magmas (Kelemen et al. 2004) that later may evolve towards more differentiated rocks by FC or AFC processes (Hawkesworth et al. 1979; Arculus and Powell 1986; Davies and Stevenson 1992; Tatsumi and Eggins 1995; Schmidt and Poli 1998; Ulmer 2001; Grove et al. 2002; Forneris and Holloway 2003).

High-K andesites and dacites analyzed in this study exhibit regular variations in major and trace element abundances indicating that fractional crystallization processes exert a major role in their genesis. In addition, Sr, Nd, Pb and Hf isotopes show significant correlations among each other but also with K_2O abundances, further implying a contribution of crustal rocks through AFC processes and addition of sediment-derived slab melts to the source of these rocks. Regular variations of fluid-sensitive trace elements such as Ba and Pb show that involvement of a fluid phase also contributed to the geochemical composition. Hf–Nd isotope decoupling suggests assimilation of aged garnet-bearing lithologies, likely Hercynian lower crustal rocks. It is obvious that the composition of the alpine andesites and dacites is not the result of a single-stage process and it is, therefore, proposed that after partial melting in a metasomatized mantle wedge, which produced unexposed high-K basalts (i.e., Hürlimann et al. 2016) and basaltic andesites, further evolution of the andesites and dacites took place in the arc crust. Here, they might have crystallized ultramafic cumulates (dunites, wehrlites, pyroxenites, hornblendites, opx-hornblendites; e.g., Müntener et al. 2021; Jagoutz et al. 2009; Hürlimann et al. 2016; Pfänder et al. 2021) and possibly promoted partial melting of the lower crust which, depending on the maturity of the crust, may consist of a mixture of meta-igneous (Hercynian and Permian intrusive rocks; Boriani et al. 1995; Pinarelli et al. 1993, 2002) and metasedimentary rocks (Hercynian amphibolite- to granulite-facies metasedimentary rocks; Schnetger 1994;

Voshage et al. 1987, 1990). This view is in accordance with the AFC model that has been used to explain the coupling of elemental and isotopic composition of the andesites and dacites from this study. Therefore, the chemical diversity of the studied andesites and dacites is, at least in part, acquired in the lower crust through complex AFC processes involving Hercynian or pre-Hercynian lower garnet-bearing crustal lithologies. Subsequent later stage magma differentiation at lower pressures in higher crustal levels involving plagioclase is suggested by decreasing CaO and Al_2O_3 with increasing SiO_2 (Fig. 2) as well as by slightly negative Eu anomalies (Fig. 4). Presumably, this differentiation was the final process that produced these andesites and dacites, which are thus end products of a process chain that might be representative for the formation of primary continental crust in continental arcs.

Older works (i.e., Beccaluva et al. 1979) have tried to explain the complex geochemical composition of andesites from the Alpine chain as a result of partial melting of quartz eclogite in the down-going slab, followed by reaction with the upper mantle wedge and low-pressure crystal fractionation at crustal levels. These authors also showed the existence of andesites with elevated MgO, Ni and Cr abundances and emphasized a role for distinct primary melts that followed different evolutionary lines. Others (Dal Piaz 1979; Beccaluva et al. 1983) noted distinct parental sources with compositional differences and strengthen a role for a metasomatized subcontinental lithospheric mantle especially for the generation of the LILE- and LREE-enriched high-K andesites and shoshonites. Mantle metasomatism (or mantle contamination) could have been achieved by subduction of continental material accompanied by fluid release during high-pressure transformation (Dal Piaz et al. 1979; von Blanckenburg et al. 1992). Such a process may explain LILE enrichment, elevated $^{87}Sr/^{86}Sr$ and radiogenic Pb isotope compositions. However, other evidences (high $\delta^{18}O$ values, radiogenic $^{87}Sr/^{86}Sr$, negative εNd values, radiogenic Pb isotopes and correlation among these isotope systems) are rather indicative of crustal contamination; a significant process proposed by Beccaluva et al. (1983), Venturelli et al. (1984), Dal Piaz (1988) and von Blanckenburg et al. (1992) for the modification of some andesites and shoshonites from the northwestern and southern Alps.

The Hf isotope compositions reported here also shed new light on the compositions of andesites in the Alpine chain and on possible crustal constituents in the lower crust. Whole rock and zircon Hf isotope data for alpine igneous rocks (Stille and Steiger 1991) indicate a range of εHf values from + 3.4 to – 2.2 which are similar to the εHf values reported from the least contaminated andesites from this study. Pre-alpine igneous rocks have $\varepsilon Hf_{(30\ Ma)}$ values ranging from + 1.2 to – 6.8 (Schaltegger and Brack 2007), again similar to the andesites and dacites studied here. In view of the apparent AFC history of the andesites and dacites, it is not unreasonable to assume that the andesites were generated by processes similar to those that generated the alpine plutons (Stille and Steiger 1991) and interacted with lower crustal Hercynian garnet-bearing metasedimentary rocks or Hercynian igneous rocks (Schaltegger and Brack 2007) during ascent.

The alpine orogen is distinct from other common subduction-related orogens worldwide. Notable features are the inferred existence of narrow ocean basins of about 400–700 km width, slow-spreading heterogeneous oceanic lithosphere with no preserved volcanic arcs (Agard and Handy 2021) and distinct trench sediments relative to those deposited in common subduction zones. However, the preservation of HP-LT rocks such as blueschists and eclogites and the occurrence of common subduction-related igneous rocks with negative Nb–Ta anomalies and positive Pb anomalies in mantle-normalized multielement diagrams clearly provide a link to common (Pacific-type) subduction zones. The geochronology of the orogenic events is well constrained and involved early subduction starting around ~ 100 Ma. Continental subduction occurred from ~ 75 to 35 Ma where subducted fragments yielded peak burial dates between ~ 60 and 35 Ma. Collision of Europe and Adria started at ~ 34 Ma (Agard and Handy 2021; Berger and Bousquet 2008). These features let Agard and Handy (2021) to conclude that the preservation of the Alpine subduction record is not atypical but reflects slow closure of a short-lived, slow-spreading ocean. The absence of a magmatic arc was explained as a result of insufficient water transfer from the slab to the infertile asthenospheric mantle or slabs too short to trigger large-scale mantle upwelling. Nevertheless, typical arc magmas are preserved but they are scarce (McCarthy et al. 2020; Müntener et al. 2021) and confined to the period between ~ 43–40 and ~ 34–30 Ma indicating a short-lived igneous history (McCarthy et al. 2018; 2021). The early products have a clear upper mantle signature whereas the late products are more evolved implying melting of ancient crustal material or assimilation of continental crust (Müntener et al. 2021). Medium to high-K rocks dominate the younger spectrum as a result of episodic fluid fluxes late in the orogenic history. Elevated $^{87}Sr/^{86}Sr$ and high LILE of these late volcanic products are explained by partial melting of a metapelitic sediment. These high-K magmas were generated during the initial stages of continental collision between ~ 34 and 30 Ma which is in full accordance with the Ar–Ar data presented here. The inferred presence of appreciable amounts of fluids would then come from hydrated subduction mantle rocks (serpentinites; McCarthy et al. 2018; 2020) to prime the mantle wedge and this is in accordance with the trace element signatures of the andesites and dacites studied here, notably their moderate high Ba/Nb and Ba/Th ratios. The presence of melts from

sedimentary rocks played also a crucial role in shaping the trace element composition, notably elevated Th/Nb, Th/La and Th/Yb and was, at least partly, also responsible for the evolved isotope composition of the andesites and dacites, in particular with respect to radiogenic Pb isotope signatures. Therefore, this study again emphasizes the view that generation of high-K magmas requires a component of partial melt from subducted sediments (Hermann and Spandler 2008; Müntener et al. 2021). In addition, AFC processes contributed to the evolved isotope compositions and contributed to elevated K_2O and evolved Sr and Nd isotope compositions (Callegari et al. 2004; Owen 2008; Müntener et al. 2021). To solve the apparent problems in explaining the unusual subduction features of the Alps, McCarthy et al. (2020) renewed the process of an A-type (Ampferer-type) subduction. Here, continental subduction involves closure of small continental basins, subduction initiation without magmatism, minor involvement of oceanic crust and subduction of dry lithosphere into the convective mantle. This elegant model can also explain the crustal signature (radiogenic $^{87}Sr/^{86}Sr$, high LILE, low HFSE, high $\delta^{18}O$, radiogenic Pb isotopes) of the late orogenic andesites studied here. In summary, to reconcile the apparent contradiction of typical arc lavas with negative Nb–Ta anomalies but crustal-like isotope features, continental arc magmatism in the Alps originated from limited flux-melting of a metasomatized mantle wedge that underwent specific enrichments during aqueous fluid and sediment-derived melt additions during Ampferer-type subduction. Primary magmas, some of them with a high-K nature developed by multiple FC and AFC processes (i.e., Hürlimann et al. 2016) within different levels of an arc crust towards high-K andesites and dacites. Most likely, Hercynian lower crustal rocks or Permian igneous rocks with radiogenic Sr and Pb but unradiogenic Nd and Hf isotope compositions played a key role during late-stage AFC processes.

Supplementary Information The online version contains supplementary material available at https://doi.org/10.1007/s00410-022-01983-w.

Acknowledgements W. S. Vogler (Universität Marburg) initiated this study in 1994 and C. Jung (Universität Marburg) performed the major element analyses. Unfortunately, both decided not to work further on this project. A. W. Hofmann (Max-Planck-Institut für Chemie, Mainz) is thanked for hospitality and for giving access to the mass spectrometry facilities. We appreciate the detailed comments of an anonymous reviewer and Anders McCarthy who helped to focus on the paper. We especially thank Anders McCarthy to bring unrecognized literature to our attention. The editor Hans Keppler is thanked for patient editorial handling of the manuscript.

Funding Open Access funding enabled and organized by Projekt DEAL.

Data availability The dataset generated and analyzed during the current study are available from the corresponding author on request.

Declarations

Conflict of interest The authors declare they have no financial interests. The authors have no competing interests to declare that are relevant to the content of this article.

References

Adam J, Green T (2006) Trace element partitioning between mica- and amphibole-bearing garnet lherzolite and hydrous basanitic melt: 1. Experimental results and the investigation of controls on partitioning behavior. Contrib Mineral Petrol 152:1–17

Agard P, Handy MR (2021) Ocean subduction dynamics in the Alps. Elements 17:9–16

Antignano A, Manning CE (2008) Rutile solubility in H_2O, H_2O–SiO_2, and H_2O–$NaAlSi_3O_8$ fluids at 0.7–2.0 GPa and 700–1000 C: implications for mobility of nominally insoluble elements. Chem Geol 255:283–293

Arculus RJ, Powell R (1986) Source component mixing in the regions of arc magma generation. J Geophys Res 91:5913–5926

Asprey LB (1976) The preparation of very pure fluorine gas. J Fluor Chem 7:359–361

Audétat A, Keppler H (2005) Solubility of rutile in subduction zone fluids, as determined by experiments in the hydrothermal diamond anvil cell. Earth Planet Sci Lett 232:393–402

Bea F, Monteiro P (1999) Behavior of accessory phases and redistribution of Zr, REE, Y, Th and U during metamorphism and partial melting of metapelites in the lower crust: an example from the Kinzingite Formation of Ivrea-Verbano, NW Italy. Geochim Cosmochim Acta 63:1133–1153

Beccaluva L, Gatto GO, Gregnanin A, Piccirillo EM, Scolari A (1979) Geochemistry and petrology of dyke magmatism in the Alto Adige (Eastern Alps) and ist geodynamic implications. N Jahrb Geol Paläo Mh 6:321–339

Beccaluva L, Bigioggero B, Chiesa S, Colombo A, Fanti G, Gatto GO, Gregnanin A, Montrasio A, Piccirillo EM, Tunesi A (1983) Post collisional orogenic dyke magmatism in the Alps. Mem Soc Geol Italy 26:341–359

Ben Othman D, White WM, Patchett PJ (1989) The geochemistry of marine sediments, island arc magma genesis, and crust-mantle recycling. Earth Planet Sci Lett 94:1–21

Berger A, Bousquet R (2008) Subduction related metamorphism in the Alps: review of isotopic ages based on petrology and their geodynamic consequences. Geol Soc London, Spec Publ 298:117–144

Bergomi MA, Zanchetta S, Tunesi A (2015) The Tertiary dike magmatism in the southern Alps: geochronological data and geodynamic significance. Int J Earth Sci 104:449–473

Blichert-Toft J, Chauvel C, Albarede F (1997) Separation of Hf and Lu for high-precision isotope analysis of rock samples by magnetic

sector multiple collector ICP-MS. Contrib Mineral Petrol 127:248–260
Boriani A, Gibbi Origoni E, Pinarelli L (1995) Paleozoic evolution of southern alpine crust (northern Italy) as indicated by contrasting granitoid suites. Lithos 35:47–63
Brenan JM, Shaw HF, Ryerson FJ, Phinney DL (1995) Mineral-aqueous fluid partitioning of trace elements at 900 °C and 2.0 GPa: constraints on the trace element chemistry of mantle and deep crustal fluids. Geochim Cosmochim Acta 59:3331–3350
Callegari E, Cigolini C, Medot O, D'Antonio M (2004) Petrogenesis of calc-alkaline and shoshonitic post-collisional Oligocene volcanics of the cover series of the Sesia Zone, Western Italian Alps. Geodin Acta 17:1–29
Cameron AE, Smith DH, Walker RL (1969) Mass spectrometry of nanogram-size samples of lead. Anal Chem 41:525–526
Cannaò E, Agostini S, Scambelluri M, Tonarini S, Godard M (2015) B, Sr and Pb isotope geochemistry of high-pressure Alpine metaperidotites monitors fluid-mediated element recycling during serpentinite dehydration in subducion mèlange (Cima di Gagnone, Swiss Central alps). Earth Planet Sci Lett 163:80–100
Chen W, Zhang G, Ruan M, Wang S, Xiong X (2021) Genesis of intermediate and silicic magmas constrained by Nb/Ta fractionation. J Geophys Res Solid Earth. https://doi.org/10.1029/2020JB020708
Class C, Miller DM, Goldstein SL, Langmuir CH (2000) Distinguishing melt and fluid subduction components in Umnak volcanics. Aleutian Arc Geochem Geophys Geosys 1:1004. https://doi.org/10.1029/1999GC000010
Clayton RN, Mayeda TD (1963) The use of bromine pentaflouride in the extraction of oxygen from oxides and silicates for isotope analysis. Geochim Cosmochim Acta 27:43–52
Crawford AJ, Falloon TJ, Eggins S (1987) The origin of island arc high alumina basalts. Contrib Mineral Petrol 97:417–430
Cumming GL, Köppel V, Ferrario A (1987) A lead isotope study of the northeastern Ivrea Zone and the adjoining Ceneri zone (N-Italy): evidence for a contaminated subcontinental mantle. Contrib Mineral Petrol 97:19–30
Dal Piaz GV, Venturelli G, Scolari A (1979) Calc-alkaline to ultrapotassic postcollisional volcanic activity in the internal northwestern Alps. Mem Sci Geol 32:4–15
Dal Piaz GV, Del Moro A, Martin S, Venturelli G (1988) Post-collisional magmatism in the Ortler-Cevedale Massif (Northern Italy). Jb Geol Bundesanstalt Wien 131:533–551
Davidson JP (1987) Crustal contamination vs subduction zone enrichment: examples from the lesser Antilles and implications for mantle source compositions of island arc volcanic rocks. Geochim Cosmochim Acta 51:2185–2198
Davidson JP, Harmon RS (1989) Oxygen isotope constraints on the petrogenesis of volcanic arc magmas from Martinique, lesser Antilles. Earth Planet Sci Lett 95:255–270
Davidson JP, McMillan NJ, Moorbath S, Wörner G, Harmon RS, Lopez-Escobar L (1990) The Nevados de Payachata volcanic region (18° S/69° W, N. Chile), II. Evidence for widespread crustal involvement in Andean magmatism. Contrib Mineral Petrol 105:412–432
Davies JH, Stevenson DJ (1992) Physical model of source region of subduction zone volcanics. J Geophys Res 97:2037–2070
DePaolo DJ (1981) Trace element and isotopic effects of combined wallrock assimilation and fractional crystallization. Earth Planet Sci Lett 53:189–202
Deutsch A (1984) Young Alpine dykes south of the Tauern Window (Austria): a K-Ar and Sr isotope study. Contrib Mineral Petrol 85:45–57
Diethelm KH (1990) Synintrusive basische Gänge und endogene Xenolithe: Magma-Mingeling in der Bergeller Intrusion. Schweizer Mineral Petrograph Mitt 70:247–264
Ducea MN, Saleeby JB (2015) Bergantz G (2015) The architecture, chemistry and evolution of continental magmatic arcs. Annu Rev Earth Planet Sci 43:299–331
Edwards CMH, Menzies MA, Thirlwall MF, Morris JD, Leeman WP, Harmon RS (1994) The transition to potassic alkaline volcanism in island arcs: the Ringgit-Beser Complex, East Java, Indonesia. J Petrol 35:1557–1595
Eiler JM (2001) Oxygen isotope variations of basaltic lavas and upper mantle rocks. Rev Mineral 43:319–364
Ellam RM, Harmon RS (1990) Oxygen isotope constraints on the crustal contribution to the subduction-related magmatism of the Aeolian Islands, southern Italy. J Volc Geotherm Res 44:105–122
Ellam RM, Hawkesworth CJ (1988) Elemental and isotopic variations in subduction related basalts: evidence for a three-component model. Contrib Mineral Petrol 98:72–80
Elliott T (2003) Tracers of the slab. Geophys Monogr 138:23–45
Elliott T, Plank T, Zindler A, White W, Bourdon B (1997) Element transport from slab to volcanic front at the Mariana arc. J Geophys Res 102:14991–15019
Foley S, Tiepolo M, Vannucci R (2002) Growth of early continental crust controlled by melting of amphibolite in subduction zones. Nature 417:837–840
Forneris JF, Holloway JR (2003) Phase equilibria in subducting basaltic crust, implications for H_2O release from the slab. Earth Planet Sci Lett 214:187–201
Gale A, Dalton CA, Langmuir CH, Su Y, Schilling J-G (2013) The mean composition of ocean ridge basalts. Geochem Geophys Geosyst 14:489–518
Gamble J, Woodhead J, Wright I, Smith I (1996) Basalt and sediment geochemistry and magma petrogensis in a transect from oceanic island arc to rifted continental margin arc: the Kermadec-Hikirangi margin. J Petrol 37:1523–1546
Gautschi A, Montrasio A (1978) Die andesitisch-basaltischen Gänge des Bergeller Ostrandes und ihre Beziehung zur Regional- und Kontaktmetamorphose. Schweiz Mineral Petrograph Mitt 58:329–343
Gehler A, Tütken T, Pack A (2012) Oxygen and carbon isotope variations in a modern rodent community - implications for palaeoenvironmental reconstructions. PLoS ONE 7(11):e49531. https://doi.org/10.1371/journal.pone.0049531
Gelati R, Napolitano A, Valdisturlo A (1988) La Gonfolite Lombarda: Stratigrafia e significato evoluzione del margine sudalpino. Riv Ital Palaeontol Stratigafia 94:285–332
Gertisser R, Keller J (2003) Trace element and Sr, Nd, Pb and O isotope variations in medium-K and high-K volcanic ricks from Merapi volcano, Central Java, Indonesia: evidence for the involvement of subducted sediments in Sunda Arc magma genesis. J Petrol 44:457–489
Gianola O, Schmidt MW, von Quadt A, Peytcheva I, Luraschi P, Reusser E (2014) Continuity in geochemistry and time of the Tertiary Bergell intrusion (Central Alps). Swiss J Geosci 107:197–222
Glazner AF (2007) Thermal limitations on incorporation of wall rock into magma. Geology 35:319–322
Gramlich JW, Murphy TJ, Garner EL, Shields WR (1973) Absolute isotope abundance ratio and atomic weight of a reference sample of rhenium. J Res Nat Bureau Stand Tech 77A:691–698
Grove TL, Harrison TM (1996) $^{40}Ar^*$ diffusion in Fe-rich biotite. Am Mineral 81:940–951
Grove TL, Kinzler RJ (1986) Petrogenesis of andesites. Ann Rev Earth Planet Sci 14:417–454
Grove TL, Gerlach DC, Sando TW, Baker MB (1983) Origin of calc-alkaline series lavas at medicine lake volcano by fractionation, assimilation and mixing. Contrib Mineral Petrol 82:407–408

Grove TL, Parman SW, Bowring SA, Price RC, Baker MB (2002) The role of an H_2O-rich fluid component in the generation of primitive basaltic andesites and andesites from the Mt. Shasta region. N California Contrib Mineral Petrol 142:375–392

Gunzenhauser BA (1985) Zur Sedimentologie und Paläogeographie der oligo-miocaenen Gonfolite Lombarda zwischen Lago Maggiore und der Brianza. Beträge zur geologischen Karte der Schweiz, 159

Harrison TM (1981) Diffusion of ^{40}Ar in hornblende. Contrib Mineral Petrol 78:324–331

Hart SR (1984) A large scale isotope anomaly in the southern hemisphere mantle. Nature 309:753–757

Hawkesworth CJ, Norry MJ, Roddick JC, Baker PE, Francis PW, Thorpe RS (1979) ^{143}Nd/^{144}Nd, ^{87}Sr/^{86}Sr, incompatible element variations in calc-alkaline andesites and plateau lavas from South America. Earth Planet Sci Lett 42:45–57

Hawkesworth CJ, Hergt JM, Ellam RM, McDermott F (1991) Element fluxes associated with subduction related magmatism. Phil Trans Roy Soc Lond 335:393–405

Hawkesworth CJ, Gallagher K, Hergt JM, McDermott F (1993) Mantle and slab contributions in arc magmas. Ann Rev Earth Planet Sci 21:175–204

Heinrichs H, Herrmann AG (1990) Praktikum der analytischen geochemie. Springer, Berlin, New York, Heidelberg

Henry P, Deloule E, Michard A (1997) The erosion of the Alps: Nd isotopic and geochemical constraints on the source of the peri-Alpine molasse sediments. Earth Planet Sci Lett 146:627–644

Hermann J, Spandler CJ (2008) Sediment melts at sub-arc depths: an experimental study. J Petrol 49:717–740

Hildreth W, Moorbath S (1988) Crustal contributions to arc magmatism in the Andes of Central Chile. Contrib Mineral Petrol 98:455–489

Hürlimann N, Müntener O, Ulmer P, Nandedkar R, Chiaradia M, Ovtcharova M (2016) Primary magmas in continental arcs and their differentiated products: Petrology of a post-plutonic dyke suite in the Tertiary Adamello Batholith (Alps). J Petrol 57:495–534

Ito E, White WM, Göpel C (1987) The O, Sr, Nd and Pb isotope geochemistry of MORB. Chem Geol 62:157–176

Jackson MG, Hart SR, Koppers AAP, Staudigel H, Konter J, Blusztajn J, Kurz M, Russel JA (2007) The return of subducted continental crust in Samoan lavas. Nature 448:684–687

Jacobsen SB, Wasserburg GJ (1980) Sm-Nd isotopic evolution of chondrites. Earth Planet Sci Lett 50:139–155

Jagoutz O (2014) Arc crustal differentiation mechanisms. Earth Planet Sci Lett 396:267–277

Jagoutz O, Kelemen PB (2015) Role of arc processes in the formation of the continental crust. Annu Rev Earth Planet Sci 43:363–404

Jagoutz OE, Burg JP, Hussain S, Dawood H, Pettke T, Iizuka T, Maruyama S (2009) Construction of the granitoid crust of an island arc part i: Geochronological and geochemical constraints from the plutonic Kohistan (NW Pakistan). Contrib Mineral Petrol 158:739

Johnson CM, Beard BL (1993) Evidence from hafnium isotopes for ancient sub-oceanic mantle beneath the Rio Grande rift. Nature 362:441–444

Jones AM, Iacumin P, Young ED (1999) High-resolution δ^{18}O analysis of tooth enamel phosphate by isotope ratio monitoring gas chromatography mass spectrometry and ultraviolet laser fluorination. Chem Geol 153:241–248

Juteau M, Michard A, Albarede F (1986) The Pb-Sr-Nd isotope chemistry of some recent circum-Mediterranean granites. Contrib Mineral Petrol 92:331–340

Kagami H, Ulmer P, Hansmann W, Dietrich V, Steiger RH (1991) Nd-Sr isotopic and geochemical characteristics of the southern Adamello (Northern Italy) intrusives: Implications for crustal versus mantle origins. J Geophys Res 96:14331–14346

Kay RW (1980) Volcanic arc magmas: implications of a melting-mixing for element recycling in the crust-upper mantle system. J Geol 88:497–522

Kelemen PB, Hanghoj K, Greene AR (2004) One view of the geochemistry of subduction-related magmatic arcs, with an emphasis on primitive Andesite and lower crust. In: Holland HD, Turekian KK (eds) Treatise on geochemistry. Elsevier, Amsterdam, pp 593–659

Keppler H (1996) Constraints from partitioning experiments on the composition of subduction-zone fluids. Nature 380:237

Kessel R, Schmidt MW, Ulmer P, Pettke T (2005) Trace element signature of subduction-zone fluids, melts and supercritical liquids at 120–180 km depth. Nature 437:724–727

Kirchenbaur M, Schuth S, Barth AR, Luguet A, König S, Idrus A, Garbe-Schönberg D, Münker C (2022) Sub-arc mantle enrichment in the Sunda rear-arc inferred from HFSE systematics in high-K lavas from Java. Contrib Mineral Petrol 177:8

Klein EM, Karsten JL (1996) Ocean-ride basalts with convergent-margin geochemical affinities from the Chile ridge. Nature 374:52–57

König S, Schuth S (2011) Deep melting of old subducted oceanic crust recorded by superchondritic Nb/Ta in modern island arc lavas. Earth Planet Sci Lett 301:265–274

Lechler PJ, Desilets MO (1987) A review of the use of loss on ignition as a measurement of total volatiles in whole rock analysis. Chem Geol 63:341–344

Lee CTA, Bachmann O (2014) How important is the role of crystal fractionation in making intermediate magmas? Insights from Zr and P systematics. Earth Planet Sci Lett 393:266–274

Lee JY, Marti K, Severinghaus JP, Kawamura K, Yoo HS, Lee JB, Kim JS (2006) A redetermination of the isotopic abundances of atmospheric Ar. Geochim Cosmochim Acta 70:4507–4512

Li Y, He J, Wang C, Santosh M, Dai J, Zhang Y, Wei Y, Wang J (2013) Late Cretaceous K-rich magmatism in central Tibet: evidence for early elevation of the Tibetian plateau? Lithos 160–161:1–13

Ludwig KR (2008) Manual for isoplot 3.7, vol 4. Berkeley Geochronology Center Special Publications, US, p 77

Mann U, Schmitt MW (2015) Melting of pelitic sediments at subarc depths: 1. Flux vs. fluid-absent melting and a parameterization of melt productivity. Chem Geol 404:150–167

Mattinson JM (1986) Geochronology of high-pressure-low temperature Franciscan metabasites. A new approach using the U-Pb system. Geol Soc Amer Mem 164:95–105

McCarthy A, Müntener O (2019) Evidence for ancient fractional melting, cryptic refertilization and rapid exhumation of Tethyan mantle (Civari Ophioloite, NW Italy). Contrib Mineral Petrol 174:69

McCarthy A, Chelle-Michou C, Müntener O, Arculus R, Blundy J (2018) Subduction initiation without magmatism: the case of the missing Alpine arc. Geology 46:1059–1062

McCarthy A, Tugend J, Mohn G, Candioti L, Chelle-Michou C, Arculus R, Schmalholz SM, Müntener O (2020) A case of Ampferer-type subduction and consequences for the Alps and the Pyrenees. Am J Sci 320:313–372

McCarthy A, Tugend J, Mohn G (2021) Formation of the Alpine orogen by amagmatic convergence and assembly of previously rifted lithosphere. Elements 17:29–34

McCulloch MT, Gamble JR (1991) Geochemical and geodynamical constraints on subduction zone magmatism. Earth Planet Sci Lett 102:358–374

McCulloch MT, Perfit MR (1981) ^{143}Nd/^{144}Nd, ^{87}Sr/^{86}Sr and trace element constraints on the petrogenesis of Aleutian island arc magmas. Earth Planet Sci Lett 56:167–179

McDermott F, Defant MJ, Hawkesworth CJ, Maury RC, Joron JL (1993) Isotope and trace element evidence for three-component mixing in the genesis of the North Luzon arc lavas (Philippines). Contrib Mineral Petrol 113:9–23

Michard A, Gurriet P, Soudant M, Albarede F (1985) Nd isotopes in French Phanerozoic shales: external vs. internal aspects of crustal evolution. Geochim Cosmochim Acta 49:601–610

Miller DM, Goldstein SL, Langmuir CH (1994) Cerium/lead and lead isotope ratios in arc magmas and the enrichment of lead in the continents. Nature 368:514–519

Morris JD, Hart SR (1983) Isotopic and incompatible element constraints on the genesis of island arc volcanics from Cold Bay and Amak Island, Aleutians, and implications for mantle structure. Geochim Cosmochim Acta 47:2015–2030

Münker C (1998) Nb/Ta fractionation in a Cambrian arc/back arc system, New Zealand: source constraints and application of refined ICPMS techniques. Chem Geol 144:23–45

Münker C (2000) The isotope and trace element budget of the Cambrian Devil River arc system, New Zealand: identification of four source components. J Petrol 41:759–788

Münker C, Weyer S, Scherer E, Mezger K (2001) Separation of high field strength elements (Nb, Ta, Zr, Hf) and Lu from rock samples for MC-ICPMS measurements. Geochem Geophys Geosys. https://doi.org/10.1029/2001GC000183

Münker C, Wörner G, Yogodzinski G, Churikova T (2004) Behaviour of high field strength elements in subduction zones: constraints from Kamchatka-Aleutian arc lavas. Earth Planet Sci Lett 224:275–293

Müntener O, Ewing T, Baumgartner LP, Manzini M, Roux T, Pellaud P, Alleman L (2018) Source and fractionation controls on subduction-related plutons and dike swarms in southern Patagonia (Torres del Paine area) and the low Nb/Ta of upper crustal igneous rocks. Contrib Mineral Petrol 173:38

Müntener O, Ulmer P, Blundy JD (2021) Superhydrous arc magmas in the alpine context. Elements 17:35–40

Myers JD, Marsh BD (1987) Aleutian lead isotope data: additional evidence for the evolution of lithospheric plumbing system. Geochim Cosmochim Acta 51:1833–1842

Nielsen SG, Marschall HR (2017) Geochemical evidence for mélange melting in global arcs. Sci Adv 3:e1602402

Nievergelt P, Dietrich V (1977) Die andesitisch-basaltischen Gänge des Piz Lizun (Bergell). Schweiz Mineral Petrograph Mitt 57:267–280

Oberli F, Meier M, Berger A, Rosenberg CL, Gieré R (2004) U-Th-Pb and $^{230}Th/^{238}U$ disequilibrium isotope systematics: precise accessory mineral chronology and melt evolution tracing in the Alpine Bergell intrusion. Geochim Cosmochim Acta 68:2543–2560

Oschidari H, Ziegler URF (1992) Vergleichende Sm-Nd und Rb-Sr-Untersuchungen an Bergeller Geröllen aus der Gonfolite Lombarda (Südalpine Molasse) und an Bergeller und Novate Granitoiden des Ursprungsgebietes. Ecl Geol Helv 85:375–384

Owen JP (2008) Geochemistry of lamprophyres from the Western Alps, Italy: implications for the origin of an enriched isotopic component in the Italian mantle. Contrib Mineral Petrol 155:341–362

Palme H, Lodders K, Jones A (2014) Solar system abundances of the elements. Treatise of geochemistry, 2nd edn. Elsevier, Netherlands, pp 15–35

Perfit MR, Gust DA, Bence AE, Arculus RJ, Taylor SR (1980) Chemical characteristics of island-arc basalts: implications for mantle sources. Chem Geol 30:227–256

Pfänder JA, Münker C, Stracke A, Mezger K (2007) Nb/Ta and Zr/Hf in ocean island basalts-Implications for crust–mantle differentiation and the fate of Niobium. Earth Planet Sci Lett 254:158–172

Pfänder JA, Sperner B, Ratschbacher L, Fischer A, Meyer M, Leistner M, Schaeben H (2014) High-resolution $^{40}Ar/^{39}Ar$ dating using a mechanical sample transfer system combined with a high-temperature cell for step heating experiments and a multi-collector ARGUS noble gas mass spectrometer. Geochem Geophys Geosys 15:1–14

Pfänder JA, Jochum KP, Galer SJG, Hellebrand EWG, Jung S, Kröner A (2021) Geochemistry of ultramafic and mafic rocks from the northern Central Asian Orogenic Belt (Tuva, Central Asia) - constraints on lower and middle arc crust formation linked to late Proterozoic intra-oceanic subduction. Prec Res 356:106061

Pinarelli L, Boriani A, Del Moro A (1993) The Pb isotope systematics during crustal contamination of subcrustal magmas: the Hercynian magmatism in the Serie dei Laghi (southern Alps, Italy). Lithos 31:51–61

Pinnarelli L, del Moro A, Boriani A, Caironi V (2002) Sr, Nd isotope evidence for an enriched mantle component in the origins of the Hercynian gabbro-granite series of the "Serie dei Laghi" (southern Alps, NW Italy). Eur J Min 14:403–415

Plank T, Langmuir CH (1998) The geochemical composition of subducting sediment and its consequences for the crust and mantle. Chem Geol 145:325–394

Plank T, White WM (1995) Nb and Ta in arc and mid-ocean basalts. AGU fall meeting abstracts. Eos 76(46):655

Price RC, Stewart RB, Woodhead JD, Smith IEM (1999) Petrogenesis of high-K arc magmas: evidence from Egmont volcano, North Island, New Zealand. J Petrol 40:167–197

Renne PR, Mundil R, Balco G, Min K, Ludwig KR (2010) Joint determination of ^{40}K decay constants and $^{40}Ar^{*}/^{40}K$ for the Fish Canyon sanidine standard, and improved accuracy for $^{40}Ar/^{39}Ar$ geochronology. Geochim Cosmochim Acta 74:5349–5367

Reubi O, Blundy J (2009) A dearth of intermediate melts at subduction zone volcanoes and the petrogenesis of arc andesites. Nature 461:1269–1273

Rogers G, Hawkesworth CJ (1989) A geochemical traverse across the North Chilean Andes: evidence for crust generation from the mantle wedge. Earth Planet Sci Lett 91:271–285

Rudnick RL, Gao S (2004) Composition of the continental crust. In: Holland HD, Turekian KK (eds) Treatise on geochemistry, vol 3. Elsevier, Amsterdam, pp 1–64

Ruffini R, Polino R, Callegari E, Hunziker JC, Pfeifer HR (1997) Volcanic clast-rich turbidites of the Taveyanne sandstones from the Thônes syncline (Savoie, France): records for a Tertiary postcollisional volcanism. Schweiz Mineral Petrograph Mitt 77:161–174

Russel WA, Papanastassiou DA, Tombrello TA (1978) Ca isotope fractionation on the earth and other isotope system materials. Geochim Cosmochim Acta 42:1075–1090

Rustioni G, Audedat A, Keppler H (2021) The composition of subduction zone fluids and the origin of the trace element enrichment in arc magmas. Contrib Mineral Petrol 176:51

Schaltegger U, Brack P (2007) Crustal-scale magmatic systems during intracontinental strike-slip tectonics: U, Pb and Hf isotopic constraints from Permian magmatic rocks of the Southern Alps. Int J Earth Sci 96:1131–1151

Scherer EE, Münker C, Mezger K (2001) Calibration of the Lutetium-Hafnium clock. Science 293:683–687

Schmidt MW, Poli S (1998) Experimentally based water budgets for dehydrating slabs and consequences for arc magma generation. Earth Planet Sci Lett 163:361–379

Schnetger B (1994) Partial melting during the evolution of the amphibolite- to granulite-facies gneisses of the Ivrea Zone, northern Italy. Chem Geol 113:71–101

Sharp ZD (1990) A laser-based microanalytical method for the in situ determination of oxygen isotope ratios of silicates and oxides. Geochim Cosmochim Acta 54:1353–1357

Spera F, Bohrson WA (2001) Energy-constrained open-system magmatic processes I: general model and energy-constrained assimilation and fractional crystallization (EC-AFC) formulation. J Petrol 42:999–1018

Stern RJ, Jackson MC, Fryer P, Ito E (1993) O, Sr, Nd and Pb isotopic composition of the Kasuga cross-chain in the Mariana Arc: a new perspective on the K-h relationship. Earth Planet Sci Lett 119:459–475

Stille P, Steiger RH (1991) Hf isotope systematics in granitoids from the central and southern Alps. Contrib Mineral Petrol 107:273–278

Stolz AJ, Varne R, Davies GR, Wheller GE, Foden JD (1990) Magma source components in an arc-continent collision zone: the Flores-Lembata sector, Sunda arc, Indonesia. Contrib Mineral Petrol 105:585–601

Stolz AJ, Jochum KP, Spettel B, Hofmann AW (1996) Fluid- and melt-related enrichment in the subarc mantle: evidence from Nb/Ta variations in island-arc basalts. Geology 24:587–590

Sun SS, McDonough WF (1989) Chemical and isotopic systematics of oceanic basalts: implications for mantle composition and processes. In: Saunders AD, Norry MJ (eds) Magmatism in the ocean basins. Geol Soc London Spec Pub, London, pp 313–345

Tang M, Lee CTA, Chen K, Erdman M, Costin G, Jiang H (2019) Nb/Ta systematics in arc magma differentiation and the role of arclogites in continental formation. Nat Comm 10:235

Tatsumi Y, Eggins S (1995) Subduction zone magmatism. Blackwell, Oxford

Tatsumi Y, Hamilton DL, Nesbit RW (1986) Chemical characteristics of fluid phase released from a subducted lithosphere and origin of arc magmas: evidence from high-pressure experiments and natural rocks. J Volc Geotherm Res 29:293–309

Thirlwall MF, Graham AM, Arculus RJ, Harmon RS, Macpherson CG (1996) Resolution of the effects of crustal contamination, sediment subduction, and fluid transport in island arc magmas: Pb-Sr-Nd-O isotope geochemistry of Grenada, Lesser Antilles. Geochim Cosmochim Acta 60:4785–4810

Turner SJ, Langmuir CH, Katz RF, Dungan MA, Escrig S (2016) Parental arc magma composition dominantly controlled by mantle-wedge structure. Nat Geosci 9:772–776

Turner SJ, Langmuir CH, Dungan MA, Escrig S (2017) The importance of mantle wedge heterogeneity to subduction zone magmatism and the origin of EM1. Earth Planet Sci Lett 472:216–228

Ulmer P (2001) Partial melting in the mantle wedge and the role of H_2O in the genesis of mantle-derived 'arc-related' magmas. Phys Earth Planet Int 127:215–232

Venturelli G, Thorpe RS, Dal Piaz GV, Del Moro A, Potts PJ (1984) Petrogenesis of calc-alkaline, shoshonitic and associated ultrapotassic Oligocene volcanic rocks from the Northwestern Alps. Contrib Mineral Petrol 86:209–220

Vervoort JD, Patchett PJ (1996) Behavior of hafnium and neodymium isotopes in the crust: constraints from Precambrian crustally derived granites. Geochim Cosmochim Acta 60:3717–3733

Vervoort JD, Patchett PJ, Söderlund U, Baker M (2004) Isotopic composition of Yb and the determination of Lu concentrations and Lu/Hf ratios by isotope dilution using MC-ICPMS. Geochem Geophys Geosyst 5:Q11002. https://doi.org/10.1029/2004GC000271

Vogel W, Kuipers G (1987) A pre-calibrated program for geological applications. Phillips New Dev X-Ray Spectrom 11:2–8

von Blanckenburg F (1992) Combined high-precision chronometry and geochemical tracing using accessory minerals: applied to the Central-Alpine Bergell intrusion (central Europe). Chem Geol 100:19–40

von Blanckenburg F, Früh-Green G, Diethelm K, Stille P (1992) Nd-, Sr-, O-isotopic and chemical evidence for a two-stage contamination history of mantle magma in the Central. Alpine Bergell Intrusion. Contrib Mineral Petrol 110:33–45

Voshage H, Hunziker JC, Hofmann AW, Zingg A (1987) A Nd and Sr isotopic study of the Ivrea zone, Southern Alps, N-Italy. Contrib Mineral Petrol 97:31–42

Voshage H, Hofmann AW, Mazzuchelli M, Rivalenti G, Sinigoi S, Raczek I, Demarchi G (1990) Isotopic evidence from the Ivrea Zone for a hybrid lower crust formed by magmatic underplating. Nature 347:731–736

Vroon PZ, Van Bergen MJ, White WM, Varekamp JC (1993) Sr-Nd-Pb isotope systematics of the Banda arc, Indonesia: combined subduction and assimilation of continental material. J Geophys Res 98:22349–22366

Vroon PZ, Lowry D, Van Bergen MJ, Boyce AJ, Mattey DP (2001) Oxygen isotope systematics of the Banda Arc: low $\delta^{18}O$ despite involvement of subducted continental material in magma genesis. Geochim Cosmochim Acta 65:589–609

Wang S, Li X, Schertl H-P, Feng Q (2019) Petrogenesis of early Cretaceous andesite dykes in the Sulu orogenic belt. Mineralogy Petrology 113:77–97

White WM, Dupré B (1986) Sediment subduction and magma genesis in the Lesser Antilles: isotopic and trace element constraints. J Geophys Res 91:5927–5941

Willbold M, Jochum KP (2005) Multi-element isotope dilution sector field ICP-MS: a precise technique for the analysis of geological materials and its application to geological reference materials. Geost Geoanal Res 29:63–82

Willbold M, Jochum KP, Raczek I, Amini MA, Stoll B, Hofmann AW (2003) Validation of multi-element isotope dilution ICPMS for the analysis of basalts. Anal Bioanal Chem 377:117–125

Woodhead J, Eggins S, Gamble J (1993) High field strength and transition element systematics in island arc and back-arc basin basalts: evidence for multi-phase melt extraction and a depleted mantle wedge. Earth Planet Sci Lett 114:491–504

Woodhead JD, Hergt JM, Davidsoan JP, Eggins SM (2001) Hafnium isotope evidence for 'conservative' element mobility during subduction zone processes. Earth Planet Sci Lett 192:331–346

Woodhead J, Hergt J, Giuliani A, Phillips D, Maas R (2017) Tracking continental-scale modification of the Earth's mantle using zircon megacrysts. Geochem Perspect Lett 4:1–6

Zernack AV, Price RC, Smith IEM, Cronin SJ, Stewart RB (2012) Temporal evolution of a high-K andesitic magmatic system: Taranaki Volcano, New Zealand. J Petrol 53:325–363